



1996-09

Wideband signal analysis for electromagnetic transient waveforms

Tummala, Murali

Monterey, California. Naval Postgraduate School

<http://hdl.handle.net/10945/24414>



Calhoun is a project of the Dudley Knox Library at NPS, furthering the precepts and goals of open government and government transparency. All information contained herein has been approved for release by the NPS Public Affairs Officer.

Dudley Knox Library / Naval Postgraduate School
411 Dyer Road / 1 University Circle
Monterey, California USA 93943

<http://www.nps.edu/library>

NPS-EC-96-013

NAVAL POSTGRADUATE SCHOOL Monterey, California



Wideband Signal Analysis for Electromagnetic Transient Waveforms

by

Murali Tummala
Soonho Jeong

September 1996

Approved for public release; distribution is unlimited.

Prepared for: Naval Air Warfare Center
Patuxent River, MD 50607-5000

Naval Postgraduate School
Monterey, California 93943-5000

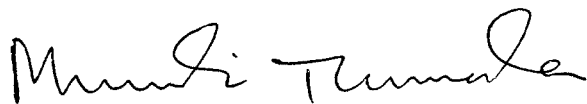
Rear Admiral M. J. Evans
Superintendent

R. Elster
Provost

This work was prepared for the Naval Air Warfare Center.

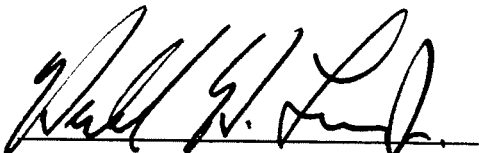
Approved for public release; distribution is unlimited.

This report was prepared by:



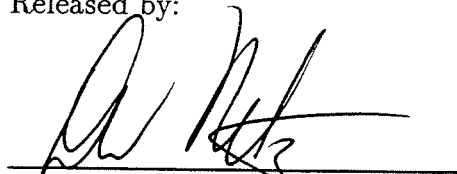
MURALI TUMMALA
Associate Professor
Department of Electrical and
Computer Engineering

Reviewed by:



HERSCHEL H. LOOMIS, JR.
Chairman,
Department of Electrical and
Computer Engineering

Released by:



DAVID W. NETZER
Associate Provost and Dean of Research



REPORT DOCUMENTATION PAGEForm Approved
OMB No. 0704-0188

Public reporting burden for the collection of information is estimated to average 1 hour per response, including the time for reviewing instructions, searching existing data sources, gathering and maintaining the data needed, and completing and reviewing the collection of information. Send comments regarding this burden estimate or any other aspect of this collection of information, including suggestions for reducing this burden to Washington Headquarters Services, Directorate for Information Operations and Reports, 1215 Jefferson Davis Highway, Suite 1204, Arlington VA 22202-4302, and to the Office of Management and Budget, Paperwork Reduction Project (0704-0188), Washington DC 20503.

1. AGENCY USE ONLY (Leave blank)		2. REPORT DATE Sep. 30, 1996	3. REPORT TYPE AND DATES COVERED Preliminary Oct. 1, 1995 to Sep 30 1996	
4. TITLE AND SUBTITLE Wideband Signal Analysis for Electromagnetic Transient Waveforms			5. FUNDING NUMBERS N0042196WRR1561	
6. AUTHOR(S) Murali Tummala and Soonho Jeong				
7. PERFORMING ORGANIZATION NAME(S) AND ADDRESS(ES) Department of Electrical and Computer Engineering Naval Postgraduate School Monterey, California 93943			8. PERFORMING ORGANIZATION REPORT NUMBER NPS-EC-96-013	
9. SPONSORING/MONITORING AGENCY NAME(S) AND ADDRESS(ES) Aircraft Division Naval Air Warfare Center Patuxent River, MD 50607-5000			10. SPONSORING/MONITORING AGENCY REPORT NUMBER	
11. SUPPLEMENTARY NOTES The views expressed in this report are those of the authors and do not reflect the official policy or position of the Department of Defense or the United States Government.				
12a. DISTRIBUTION/AVAILABILITY STATEMENT Approved for public release; distribution unlimited.			12b. DISTRIBUTION CODE	
13. ABSTRACT (Maximum 200 words) This report presents the bandpass inverse fast-Fourier transform (IFFT) filter bank and the multirate digital filter bank techniques to synthesize test point waveforms from the constituent aircraft test waveforms. The constituent waveforms are recorded by two separate measurement systems (High-Powered Pulse Waveform (HPW) in the time domain and Continuous Sweep Waveform (CSW) in the frequency domain) under two different aircraft orientations (parallel and perpendicular). Data from the two orientations are combined using the sinusoidal modeling algorithm (SMA). The tree-structured filter bank with power symmetric overlap method and the bandpass IFFT with spectral concatenation method are developed to further combine these waveforms with an overlapping frequency spectrum to produce the corresponding synthesized test point waveform.				
14. SUBJECT TERMS fast Fourier transform, multirate filter banks, waveform analysis and synthesis, electromagnetic transients			15. NUMBER OF PAGES 52	
			16. PRICE CODE	
17. SECURITY CLASSIFICATION OF REPORT UNCLASSIFIED	18. SECURITY CLASSIFICATION OF REPORT UNCLASSIFIED	19. SECURITY CLASSIFICATION OF ABSTRACT UNCLASSIFIED	20. LIMITATION OF ABSTRACT SAR	

ABSTRACT

This report presents the bandpass inverse fast-Fourier transform (IFFT) filter bank and the multirate digital filter bank techniques to synthesize test point waveforms from the constituent aircraft test waveforms. The constituent waveforms are recorded by two separate measurement systems (High-Powered Pulse Waveform (HPW) in the time domain and Continuous Sweep Waveform (CSW) in the frequency domain) under two different aircraft orientations (parallel and perpendicular). Data from the two orientations are combined using the sinusoidal modeling algorithm (SMA). The tree-structured filter bank with power symmetric overlap method and the bandpass IFFT with spectral concatenation method are developed to further combine these waveforms with an overlapping frequency spectrum to produce the corresponding synthesized test point waveform.

I. INTRODUCTION

Testing of aircraft for hardness evaluation involves measurement of wideband electromagnetic transient waveforms. It is difficult to devise a single measurement system for such wideband signals. As a result, wideband measurements are often performed by more than one instrument. These separate measurements covering different frequency bands are then combined together to synthesize an equivalent single waveform in both time and frequency domains. The data sets used here were collected from an aircraft hardness test. Measurements were made at specific test points inside the aircraft. Four waveforms were collected at each test point: two waveforms from the High-Powered Pulse Waveform (HPW) measurements and two waveforms from the Continuous Sweep Waveform (CSW) measurements. Each of these waveforms was obtained from either parallel or perpendicular orientation of the aircraft. The HPW data set was recorded in the time domain while the CSW was measured in the frequency domain. The two sets of measurements cover different frequency bands with a small overlap in the 80-100 MHz range. Different sampling rates were used to record the data, and the frequency domain measurements were actually recorded in six different frequency bands at varying bin widths.

The goal of this work is to develop techniques for combining component waveforms measured at a test point in the aircraft to produce a synthesized test point drive waveform. These waveforms are measured under two different orientations and over two different frequency bands. In previous work, some algorithms were designed by Winnenberg [Ref. 1] and Martin [Ref. 2] to produce synthetic signals with close statistical similarity to original signal. In this report, the bandpass IFFT and the multirate digital filter banks are employed to combine the measured data to produce a synthesized test point transient

waveform which still retains the basic properties of the component signals. There are four waveforms to be combined: two HPW and two CSW waveforms, which together encompass the spectrum from 0.5 MHz to 1 GHz.

The concept of wideband analysis as it applies to digital signal processing can be explained as a method of dividing a large frequency range into smaller, more manageable subbands [Ref. 3]. Thus, the analysis will essentially divide the original signal into groups of signals which retain the frequency characteristics of the original signal. FFT and multirate filter banks are used to perform wideband signal analysis and synthesis. Since a method of physically measuring the test point signal covering the entire spectrum of interest does not exist, it is not possible to directly determine the accuracy or effectiveness of the work presented. Therefore, the norm attributes of each signal are computed to determine the closeness of the synthesized test point signal to its component waveforms.

II. BANDPASS SIGNALS

The spectrum of bandpass signals is nonzero only within a region of $\pm W$ around some carrier (center) frequency, $f_c > W$, where $2W$ is the bandpass signal bandwidth. A bandpass signal is represented in general as

$$x(t) = A(t) \cos[2\pi f_c t + \phi(t)] \quad (2.1)$$

where $A(t)$ is the envelope of the signal, and $\phi(t)$ is the phase of the signal [Ref. 5]. The amplitude spectrum, $|X(f)|$, of a typical bandpass signal, $x(t)$, is shown in Figure 2.1(a).

The pre-envelope of the bandpass signal is defined by

$$x^\dagger(t) = x(t) + j\hat{x}(t) \quad (2.2)$$

where $\hat{x}(t)$ is the Hilbert transform of $x(t)$.

If $X^\dagger(f)$ is defined as the Fourier transform of $x^\dagger(t)$ and $\hat{X}(f)$ is defined as the Fourier transform of $\hat{x}(t)$, then

$$X^\dagger(f) = X(f) + j\hat{X}(f) \quad (2.3)$$

From Haykin [Ref. 6], it is known that $\hat{X}(f) = -j\text{sgn}(f)X(f)$, where $\text{sgn}(f)$ is the signum function. Then, Equation 2.3 may be written as

$$X^\dagger(f) = X(f) + \text{sgn}(f)X(f) \quad (2.4)$$

Using the definition of the signum function, Equation 2.4 becomes

$$X^+(f) = \begin{cases} 2X(f), & f > 0 \\ X(0), & f = 0 \\ 0, & f < 0 \end{cases} \quad (2.5)$$

where $X(0)$ is the zero frequency value of $X(f)$. From Equation 2.5, it is clear that there is no negative frequency component in the pre-envelope of a Fourier transformable signal as shown Figure 2.1(b). From the frequency shifting property of the Fourier trans

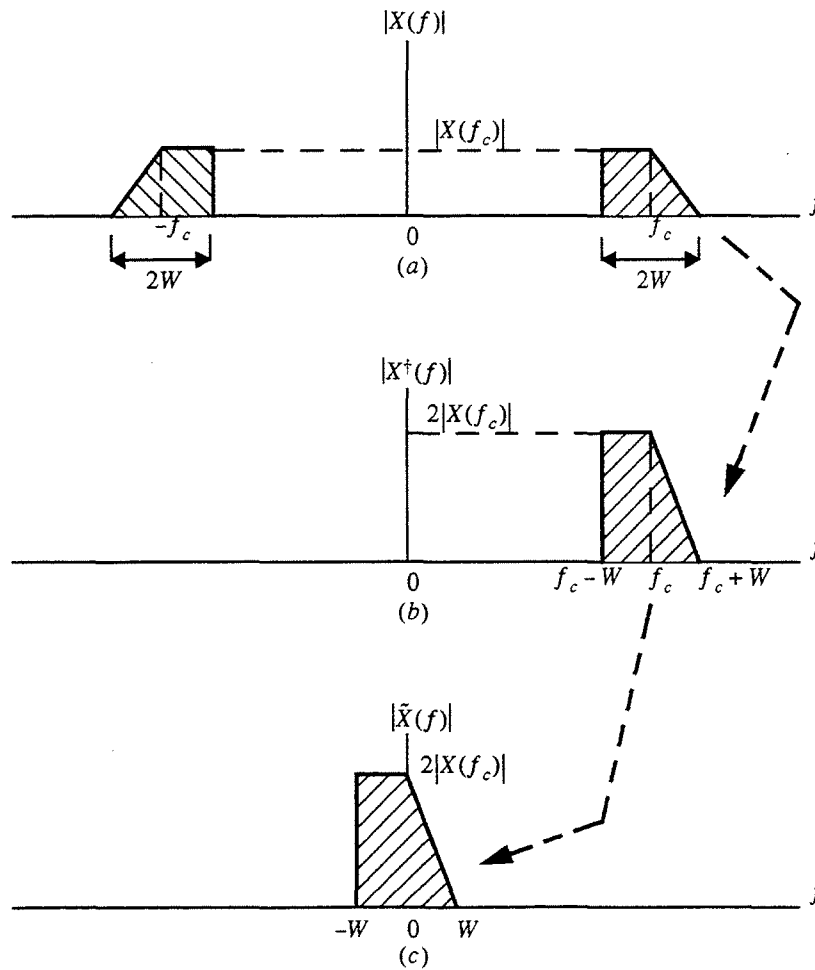


Figure 2.1: Complex Lowpass Representation of Bandpass Signals. After [Ref. 6].

form, the pre-envelope may be expressed as

$$x^\dagger(t) = \tilde{x}(t)e^{j2\pi f_c t} \quad (2.6)$$

where $\tilde{x}(t)$ is a complex-valued lowpass signal whose amplitude spectrum is shown in Figure 2.1(c). From Equation 2.6, any real bandpass signal, $x(t)$, can be represented in terms of an equivalent complex-valued lowpass signal, $\tilde{x}(t)$.

Figure 2.2 describes sampling of a bandpass signal. Consider a bandpass signal,

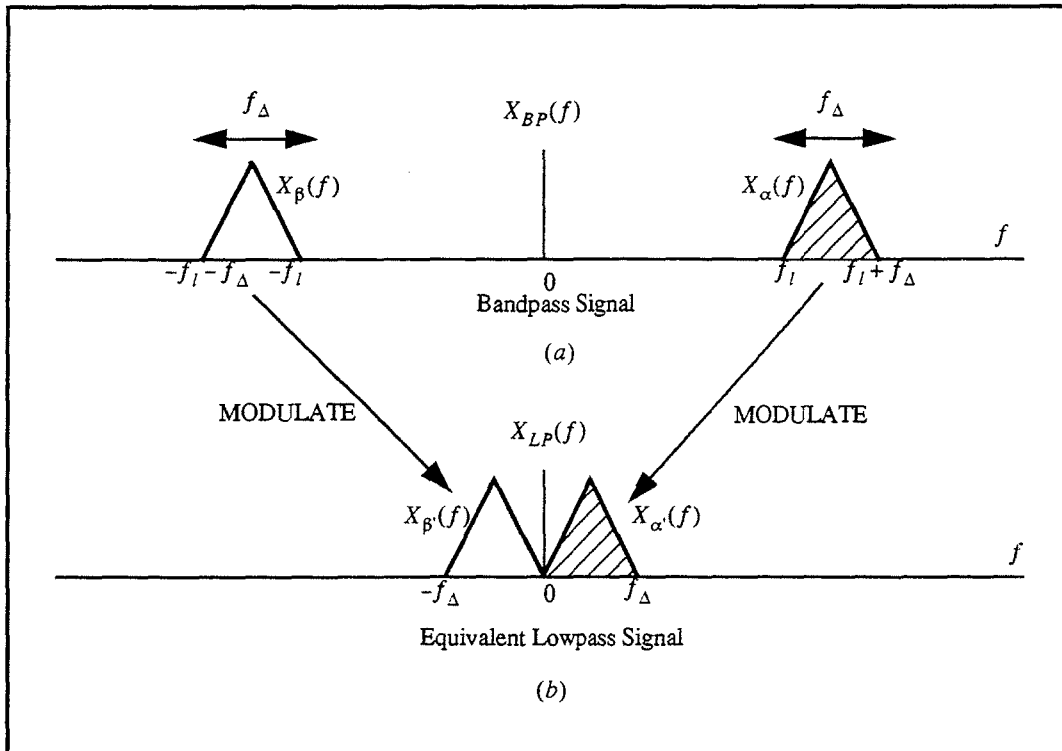


Figure 2.2: Frequency Translation of Bandpass Signals: (a) Spectrum of Bandpass Signal and (b) Its Lowpass Representation. After [Ref. 7].

$X_{BP}(f)$, which contains spectral components only in the frequency range, $f_l < |f| < f_l + f_\Delta$. Let $X_\alpha(f)$ denote the component of $X_{BP}(f)$ associated with $f > 0$ and $X_\beta(f)$ denote the component of $X_{BP}(f)$ associated with $f < 0$, as shown in Figure 2.2(a).

Figure 2.2(b) illustrates that by lowpass translating (modulating) $X_\alpha(f)$ to the band

0 to f_{Δ} and $X_{BP}(f)$ to the band $-f_{\Delta}$ to 0, the new signal, $X_{LP}(f)$, can be generated which is “equivalent” to $X_{BP}(f)$ in the sense that $X_{BP}(f)$ can be uniquely reconstructed from $X_{LP}(f)$ by the inverse process of bandpass translation. However, by applying the concept of lowpass filtering, it can be shown that the sampling frequency required to represent this is now $f_{sLP} \geq 2f_{\Delta}$, which can be much less than $f_{sBP} \geq 2(f_l + f_{\Delta})$.

In practice, there are many ways in which the combination of frequency translation and sampling described above can be performed. Several modulation techniques including integer-band sampling, quadrature modulation, and single sideband modulation are described in [Ref. 7].

1. Inverse-Fourier Transform of Bandpass Signals

Each subband signal of the CSW waveform was actually recorded at a different sampling rate with no measurements for negative frequencies. This signal may be considered a pre-envelope of a bandpass signal which is Fourier transformable. Let $s(t)$ be one of the subband signals of the CSW waveform, which is recorded in the frequency domain. Because there is no data available on the negative frequency side, we handle this signal as $s^{\dagger}(t)$, which is a pre-envelope of $s(t)$. The amplitude spectrum, $|S^{\dagger}(f)|$, of this signal is depicted in Figure 2.3(a).

From the inverse processes of Equations 2.2, 2.3, and 2.6, we can obtain the subband signal in the frequency domain as depicted in Figures 2.3(a), (b) and (c). Figure 2.3(c) shows the spectra after zero-padding. This signal can be inverse Fourier signal is depicted in Figure 2.3(a).transformed to obtain the corresponding time domain signal for further analysis. These steps can be interpreted as a bandpass IFFT operation (see Figure 2.3(d)).

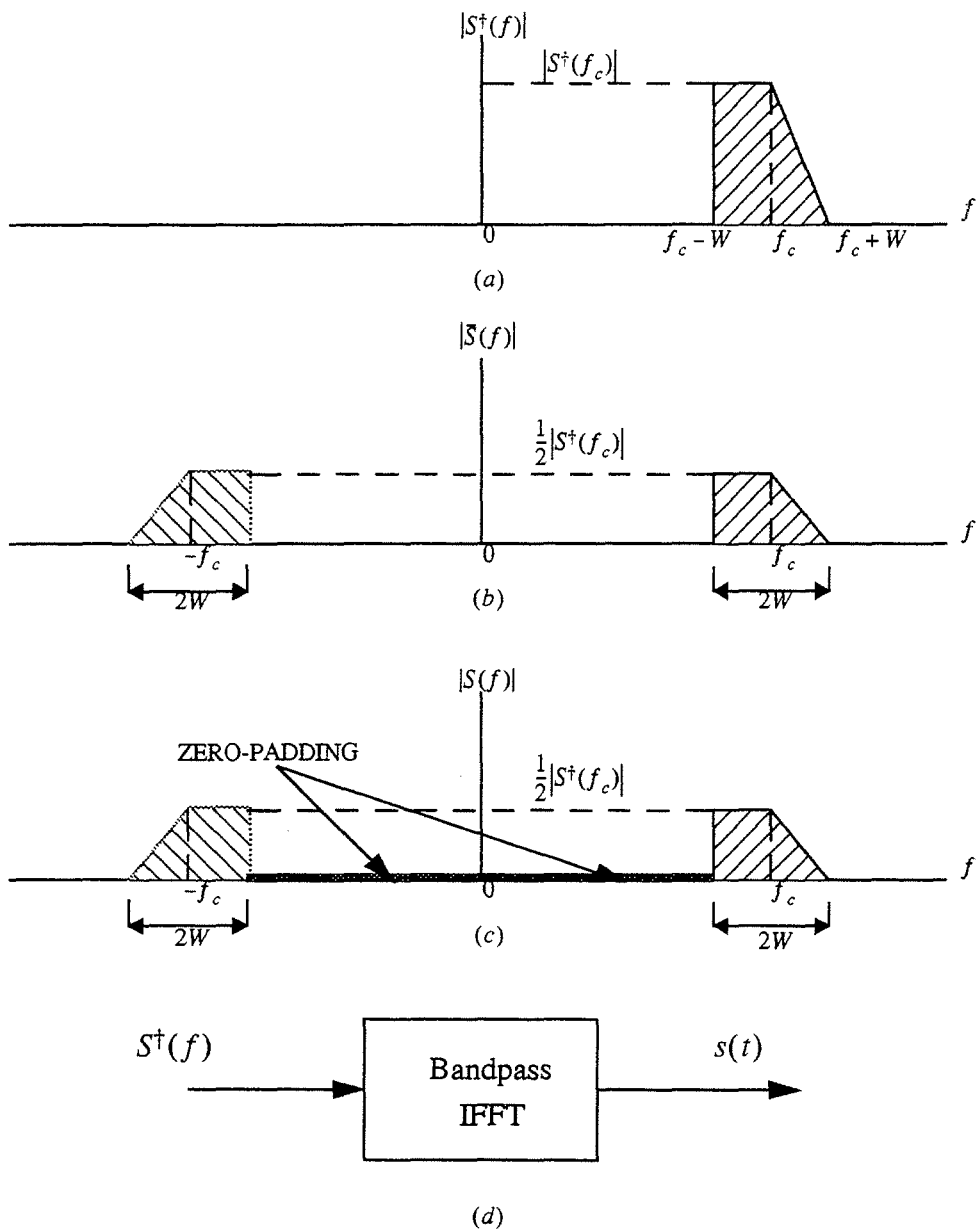


Figure 2.3: Transformation of a Bandpass Signal from the Frequency-Domain to the Time-Domain.

Figure 2.4 shows a typical CSW waveform, which is recorded in the frequency domain. As was mentioned earlier, different sampling rates were used in each subband as shown in Figure 2.5. Each subband signal is needed to be interpolated and/or decimated

to realize the overall CSW waveform with a constant sampling rate.

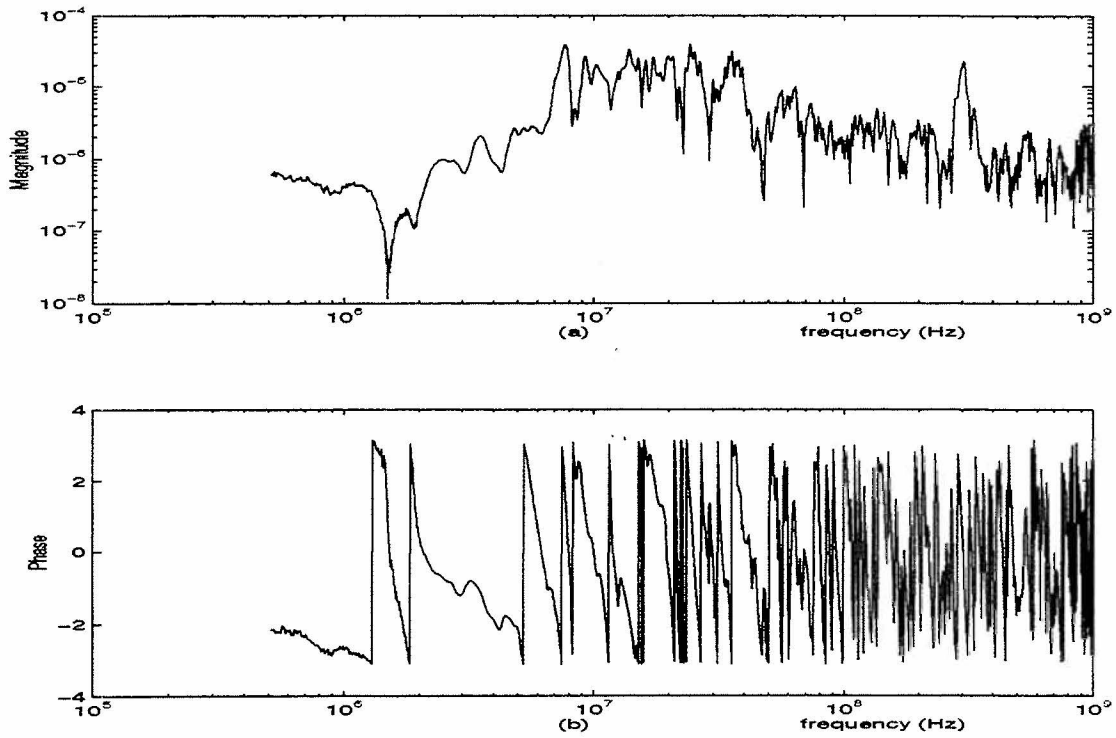


Figure 2.4: Magnitude and Phase Measurements of a CSW Waveform (LAI01001).

Let $\Delta f_1, \Delta f_2, \dots, \Delta f_6$, be the frequency bin widths of subband signals, S_1, S_2, \dots, S_6 , respectively, as shown in Figure 2.5. Table 2.1 shows the frequency ranges and bin widths of the six subband signals of the CSW waveform.

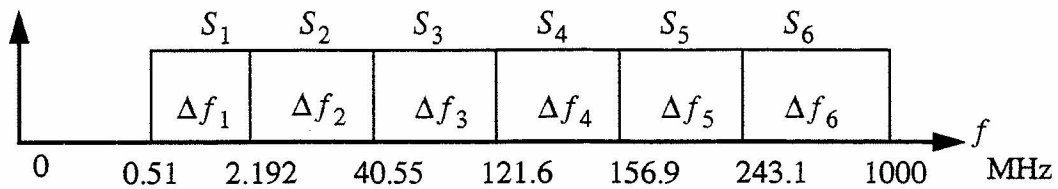


Figure 2.5: CSW Subbands

Table 1: Subband Frequency Ranges and Bin Widths of Test Data

Subband Signal	Frequency Band (Hz)	Bin Width (Hz)
S_1	0.510e6 - 2.192e6	0.0847e5
S_2	2.192e6 - 40.55e6	0.3651e5
S_3	40.55e6 - 121.6e6	6.7375e5
S_4	121.6e6 - 159.6e6	19.500e5
S_5	159.6e6 - 243.1e6	26.060e5
S_6	243.1e6 - 1000e6	40.476e5

Let N_1, N_2, \dots, N_6 be the number of sampled data points of subband signals S_1, S_2, \dots, S_6 , respectively. Subband signals S_2-S_6 are interpolated to achieve a uniform bin width of $\Delta f = \Delta f_1$ as shown in Figure 2.6. Table 2.2 includes the interpolation factors used to obtain the uniform bin width for all subbands. Note that N_1 does not change as S_1 is not modified. With the change in the bin width, the corresponding data points in subbands S_2-S_6 can be expressed as

$$N_n' = N_n \times \frac{\Delta f_n}{\Delta f_1} \quad (2.7)$$

where N_n' is the new number of data points, Δf_n is the original bin width of subband signal S_n , for $n=2, 3, \dots, 6$, and Δf_1 is the frequency bin width of subband signal S_1

The total data number of points in the frequency domain, N_{total} , after the bin width conversion in the subbands, is given by

$$N_{\text{total}} = N_1 + N_2' + \dots + N_6'. \quad (2.8)$$

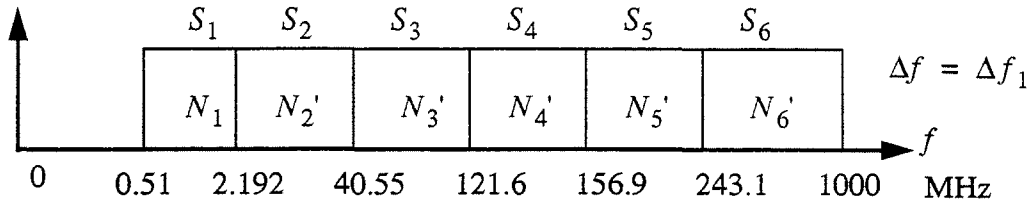


Figure 2.6: Conversion to Uniform Bin Width by Interpolation

Table 2: Subband Frequency Ranges and Interpolation Factors of Test Data

Subband Signal	Frequency Band (Hz)	Interpolation Factor
\$S_1\$	\$0.510e6 - 2.192e6\$	1
\$S_2\$	\$2.192e6 - 40.55e6\$	\$43/10\$
\$S_3\$	\$40.55e6 - 121.6e6\$	80
\$S_4\$	\$121.6e6 - 159.6e6\$	224
\$S_5\$	\$159.6e6 - 243.1e6\$	308
\$S_6\$	\$243.1e6 - 1000e6\$	478

The bin width in the frequency domain is related to the sampling frequency, f_s , and the total number of points as follows:

$$\Delta f = \frac{f_s}{2N_{\text{total}}} = \frac{1}{2N_{\text{total}}\Delta t} \quad (2.9)$$

where Δt is the corresponding sampling period in the time domain. The sampling period or the sampling frequency can, therefore, be determined as

$$\Delta t = \frac{1}{2N_{\text{total}}\Delta f} \quad \text{or} \quad f_s = 2N_{\text{total}}\Delta f \quad (2.10)$$

2. Time-Domain Representation of the CSW Waveform

Given the CSW data measured in six subbands at different bin widths, we first perform the bin width conversion to obtain a uniform bin width representation as shown in Figure 2.6. From Equation 2.10, we have the corresponding sampling period. Following on the lines of Figure 2.3, the two-sided, zero-padded CSW spectrum is obtained. An inverse Fourier transform is then performed on the spectral data to obtain the corresponding time-domain signal.

The following time-domain interpolation method is used in the rest of the report take the inverse Fourier transform of each subband without changing the bin width; interpolate subband CSW waveforms in the time domain; sum together to obtain the time domain CSW waveform. The interpolation of the subband signals in the time domain is performed such that Equation 2.10 is satisfied. The interpolation factors used in the time domain are same as those in the frequency domain (see Table 2.2).

Figures 2.7 shows the plots of the time domain CSW waveform obtained from this method. In the frequency domain, all components below 80 MHz have been discarded, which mainly leaves four subbands: part of S_3 and S_4-S_6 (see Figure 2.5).

3. Synthesis of the Wideband Waveform by Concatenation

In this section, we present methods to synthesize a single wideband signal from HPW and CSW signals originating from the same test point with overlapped frequency spectra in the region 80-100 MHz. Figure 2.8 shows a typical HPW waveform (measured in the time domain) and its magnitude spectrum.

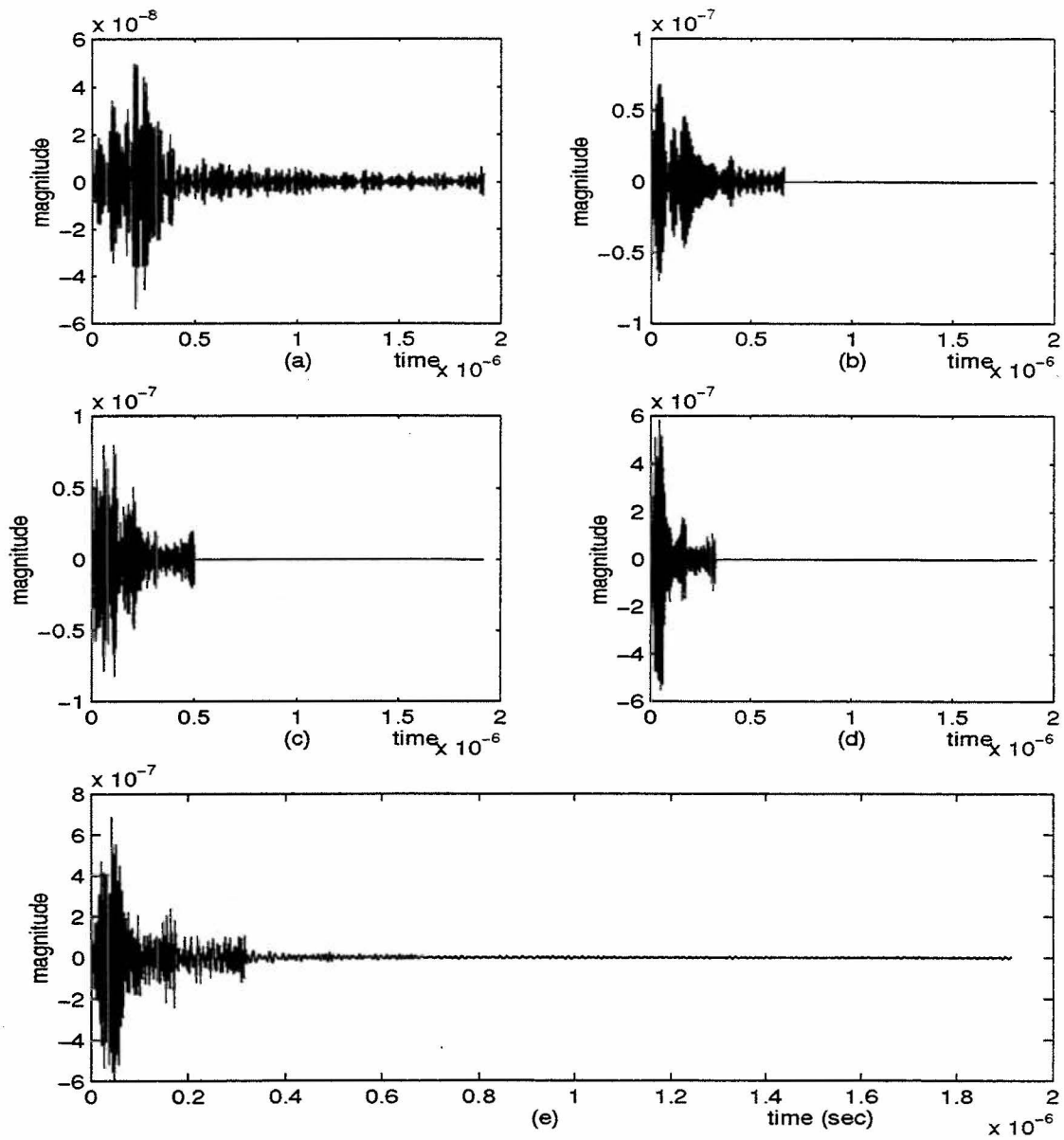


Figure 2.7: Time Domain Interpolation: (a) S_3 : 80 - 121.6 MHz. (b) S_4 : 121.6 - 156.9 MHz. (c) S_5 : 156.9 - 243.1 MHz. (d) S_6 : 243.1 - 1000 MHz. (e) Synthesis Signal of (a) - (d).

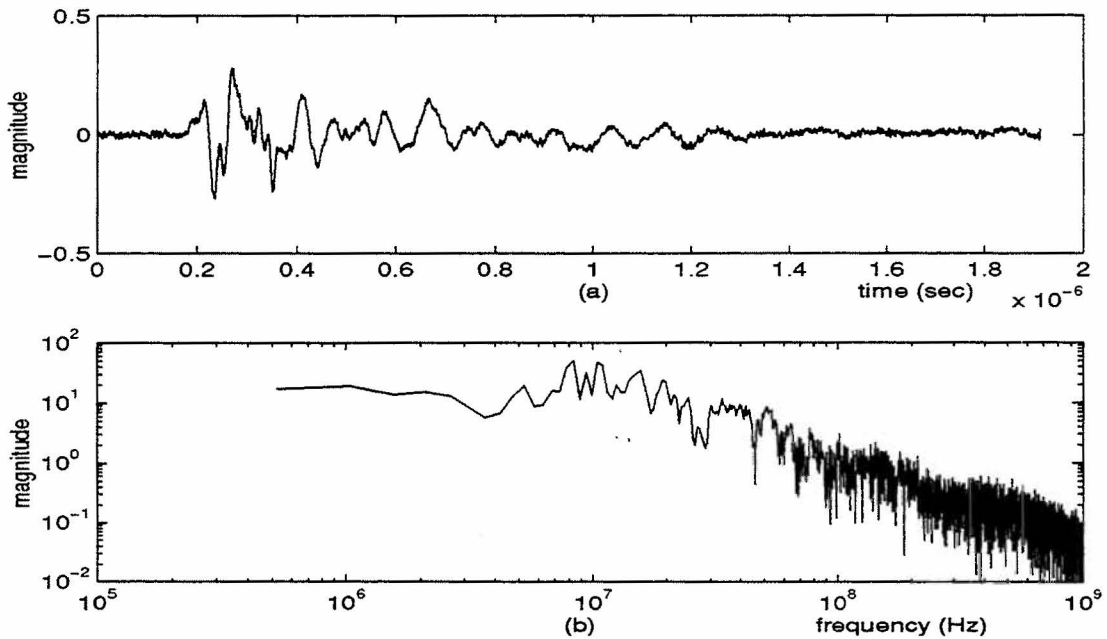


Figure 2.8: HPW Waveform (TAI01001): (a) Time Domain Representation (b) Magni-

Due to the dynamic range and analog bandwidth limitation of the HPW data, the frequency content of the HPW waveform is considered reliable only up to 100 MHz. Thus, even though higher frequency data are available, our frequency range of interest is limited to from about 0.5 MHz to 100 MHz. The HPW data were measured using a sampling rate of $f_s = 2.1394 \times 10^9$. The bin width of the HPW waveform is $\Delta f_T = 5.223 \times 10^5$ Hz. Our goal is to merge the low frequency HPW and the high frequency CSW to obtain a single waveform covering the frequency range from 0.5 MHz to 1 GHz. The CSW phase measurements may be inaccurate below 80 MHz. This prevents our obtaining the low frequency waveform from CSW data alone. Figure 2.9 shows the magnitude spectra of both HPW (TAI01001) and CSW (LAI01001) waveforms which were collected from the same test point (I01001) in parallel (A) orientation.

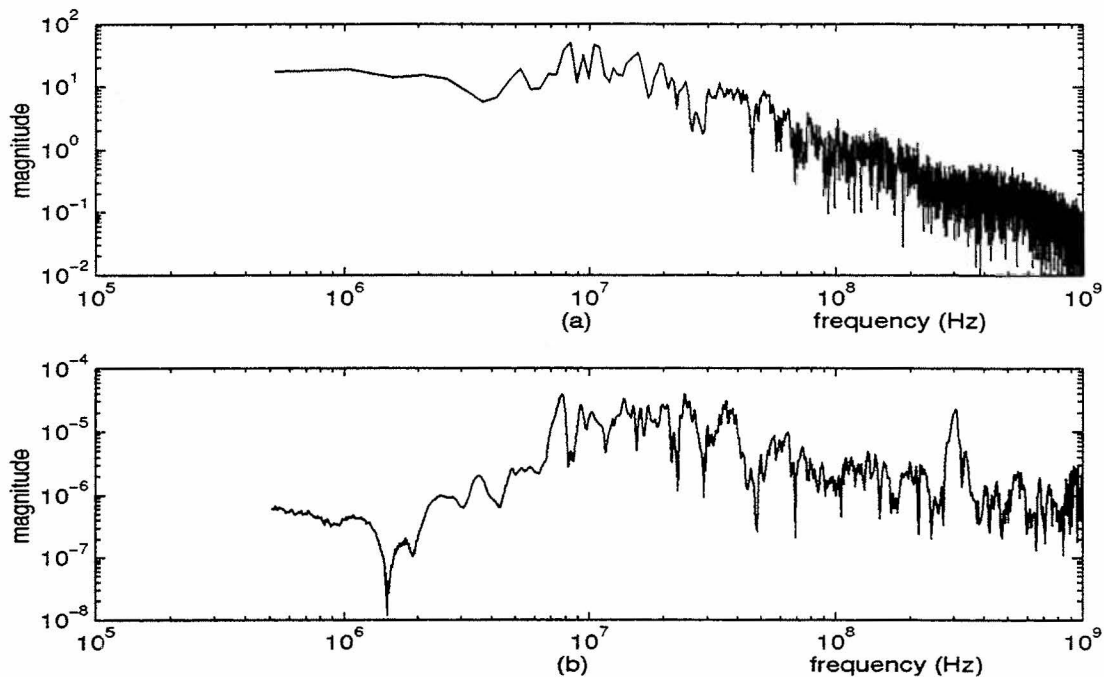


Figure 2.9: Magnitude Spectrum of (a) HPW Waveform (TAI01001) and (b) CSW Waveform (LAI01001).

The HPW and CSW waveforms are truncated, leaving an overlapped region 80 - 100 MHz. Figure 2.10 shows the truncated and overlapped spectra of HPW and CSW waveforms. Frequency components from 100 to 1000 MHz of TAI01001 and frequency components from 0.51 to 80 MHz of LAI01001 were discarded. Prior to concatenation and inverse-Fourier transform of the combined spectrum, the bin width of all the subbands including that of the HPW have to be the same. Table 2.3 shows the frequency ranges, bin width and interpolation/decimation factors needed to achieve a uniform bin width. Then a two-sided spectrum is formed, and the time domain representation of the combined signal is obtained by the inverse-Fourier transform of this spectrum.

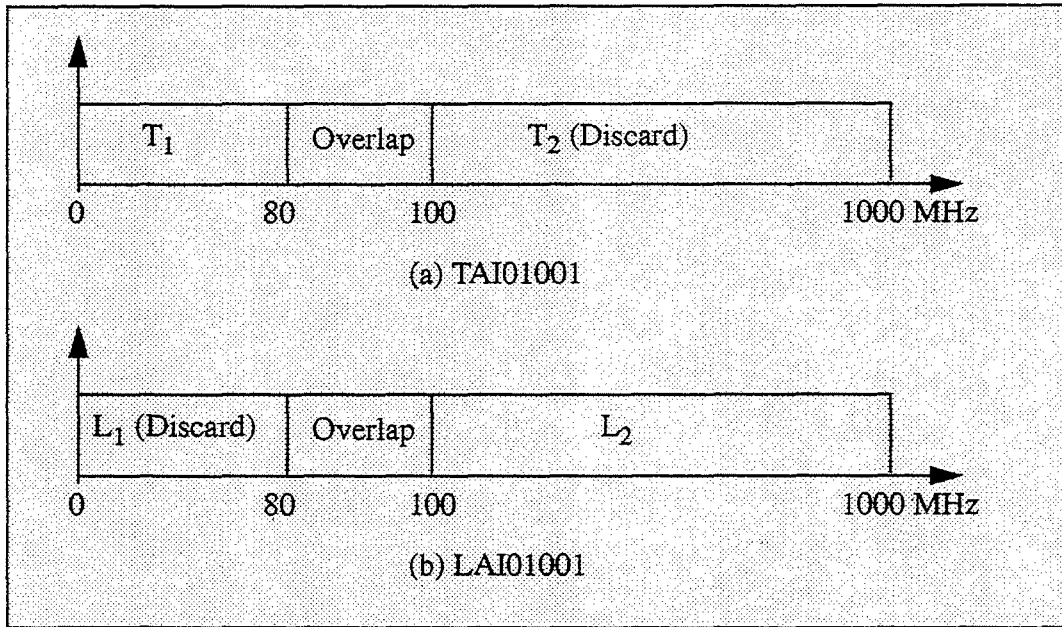


Figure 2.10: Subband Spectra: (a) HPW Waveform (TAI01001) (b) CSW Waveform

Prior to combining the CSW and HPW waveforms, the CSW data is normalized by multiplying by a constant:

$$\eta = \frac{E_T}{E_L} \quad (2.11)$$

Table 3: Subband Frequency Ranges, Bin Width and Interpolation/Decimation Factors of Test Data

Subband Signal	Frequency Range (Hz)	Bin Width (Hz)	Bin Width Conversion (Up/Down) Factor
S _T	0 - 100e6	5.2231e5	1/1
S ₁	0.510e6 - 2.192e6	0.0847e5	1/62
S ₂	2.192e6 - 40.55e6	0.3651e5	3/43

Table 3: Subband Frequency Ranges, Bin Width and Interpolation/Decimation Factors of Test Data

Subband Signal	Frequency Range (Hz)	Bin Width (Hz)	Bin Width Conversion (Up/Down) Factor
S ₃	40.55e6 - 121.6e6	6.7375e5	9/7
S ₄	121.6e6 - 159.6e6	19.500e5	15/4
S ₅	159.6e6 - 243.1e6	26.060e5	5/1
S ₆	243.1e6 - 1000e6	40.476e5	31/4

where $E_T = \sqrt{\sum_{f=80MHz}^{100MHz} T_1^2(f)}$, $E_L = \sqrt{\sum_{f=80MHz}^{100MHz} L_2^2(f)}$, and $T(f)$ represents the HPW waveform and $L(f)$ the CSW waveform.

The combined waveform, which covers the entire frequency band of the given HPW and CSW waveforms together, can be obtained as follows. The HPW spectrum up to 80 MHz is concatenated with the CSW spectrum (80 MHz to 1 GHz). Thus, the overlapped region is covered by the components of either HPW or CSW. Later, another approach to combine the spectral components over the overlapped region is detailed.

Before the spectral concatenation is carried out, the HPW and CSW waveforms have to be time aligned. From Figures 2.7(e) and 2.8(a), we notice that the HPW waveform starts to build up around 0.2 μs while the CSW begins around the origin. Since the HPW is measured in the time domain, the HPW waveform is used as a reference, and the CSW waveform is time shifted to align with the HPW waveform.

The results are shown in Figure 2.11. The sharp truncation of spectra as described in the above may lead to some spurious components in the time domain unless the amplitude of the spectrum is small enough at the truncation frequency [Ref. 6]. In Figure 2.11, however, no such components are visible. Nevertheless, any effects of truncation can be minimized by making a gentler transition to zero at the cutoff frequency through a proper

filter function. A possible disadvantage of the use of the filter function is that there is an overlap at the cutoff frequency which should be investigated.

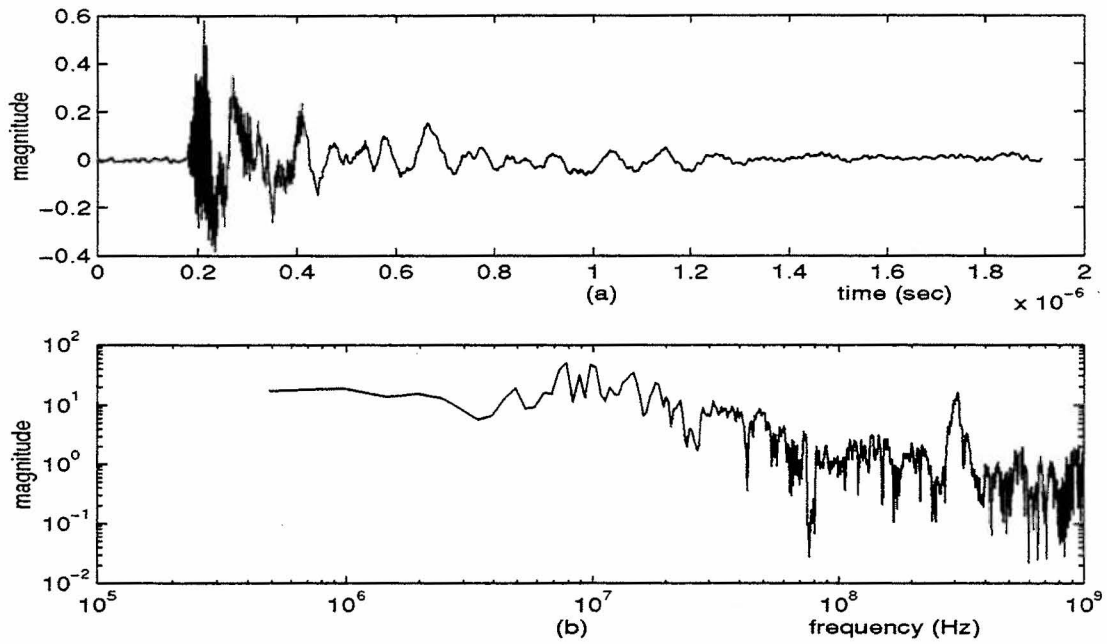


Figure 2.11: Concatenation at 80 MHz: (a) Time and (b) Frequency Representation.

III. MULTIRATE FILTER BANKS

The quadrature mirror filter (QMF) bank can be used in both analysis and synthesis banks to produce a perfect reconstruction synthesis signal [Ref. 3, 7-8]. The most well-known type of multirate filter bank is the M -channel maximally decimated QMF bank, which is shown in Figure 3.1.

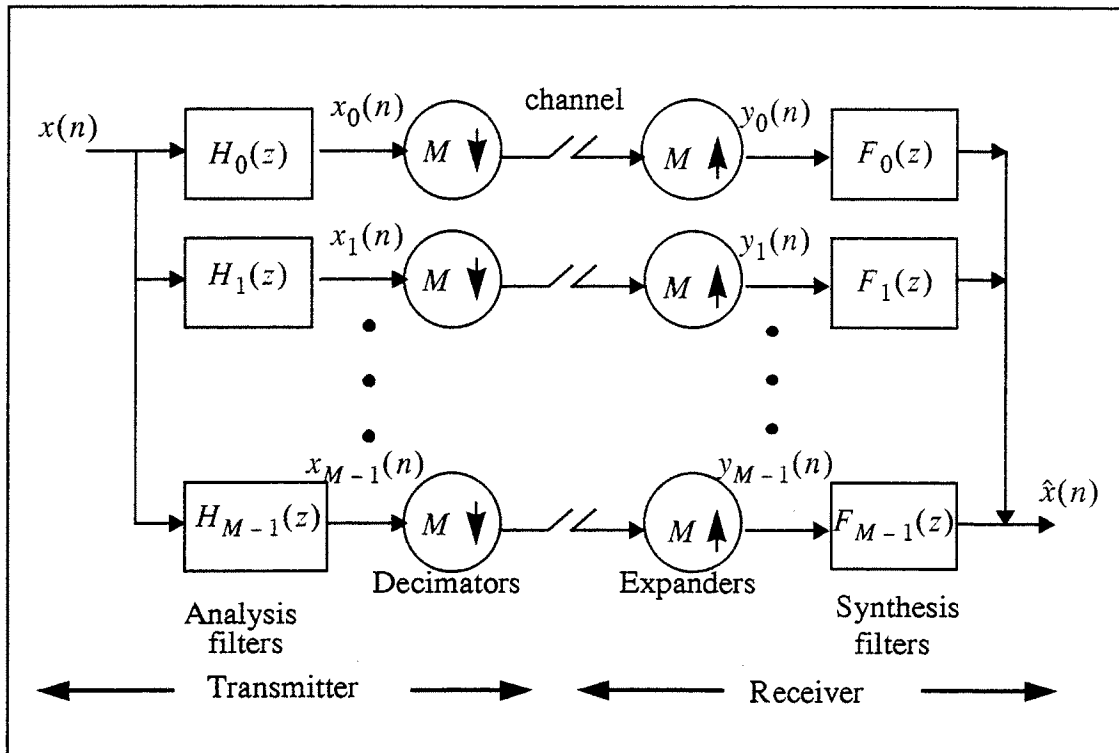


Figure 3.1 The Quadrature Mirror Filter (QMF) Bank. After [Ref. 3].

The reconstructed signal, $\hat{x}(n)$, in general suffers from aliasing error because the analysis bank filters, $H_k(z)$, that precede the decimators are not ideal. However, in practice, for a given set of analysis filters, $H_k(z)$, the synthesis filters, $F_k(z)$, can be chosen to reduce the effect of the aliasing caused by the decimation operation.

The most general expression for $\hat{X}(z)$ is of the form [Ref. 3]

$$\hat{X}(z) = \frac{1}{M} \sum_{l=0}^{M-1} X(zW^{-l}) \sum_{k=0}^{M-1} H_k(zW^{-l}) F_k(z) \quad (3.1)$$

where $X(zW^{-l}) = X(z e^{(-j\pi l)/M})$, $l \neq 0$ represents the aliasing terms. If we consider a two channel ($M=2$) filter bank, this expression can be rewritten as

$$\begin{aligned} \hat{X}(z) = & \frac{1}{2} [H_0(z)F_0(z) + H_1(z)F_1(z)]X(z) \\ & + \frac{1}{2} [H_0(-z)F_0(z) + H_1(-z)F_1(z)]X(-z) \end{aligned} \quad (3.2)$$

where $X(-z)$ corresponds to $X(e^{j(\pi-\omega)})$ on the unit circle. The frequency response of the two channel filter bank is represented by the first term in Equation 3.2 while the second term represents the aliasing. To obtain aliasing cancellation, the analysis and synthesis filters must be selected so that the quantity of the second term is zero:

$$\begin{aligned} F_0(z) &= H_1(-z) \\ F_1(z) &= -H_0(-z). \end{aligned} \quad (3.3)$$

Therefore, once the analysis filters, $H_0(z)$ and $H_1(z)$, are given, it is possible to completely cancel aliasing by the choice of matching synthesis filters, $F_0(z)$ and $F_1(z)$, which are lowpass and highpass respectively. Using Equation 3.3 for the aliasing cancellation conditions, Equation 3.2 becomes

$$\hat{X}(z) = \frac{1}{2} [H_0(z)F_0(z) + H_1(z)F_1(z)]X(z) = T(z)X(z) \quad (3.4)$$

where $T(z) = \frac{1}{2} [H_0(z)F_0(z) + H_1(z)F_1(z)]$. If $T(z)$ satisfies the conditions of a stable all-pass and a linear-phase FIR function, this system is free from amplitude distortion and phase distortion, respectively. Such QMF banks which are free from aliasing, amplitude and phase distortion are called perfect reconstruction (PR) banks and satisfy

$$\hat{X}(z) = cz^{-n_0}X(z) \quad \text{or} \quad \hat{x}(n) = cx(n - n_0) \quad (3.5)$$

where c is an arbitrary nonzero constant and n_0 is a positive integer [Refs. 3 and 5].

Figure 3.2 shows a general non-uniform filter bank with rational decimation factors. In this system, an input signal can be arbitrarily decomposed into a number of different non-uniform frequency subbands. For a perfect reconstruction with maximally decimated system, the decimation and interpolation factors, P_k and Q_k , $k = 0, \dots, M - 1$, satisfy the following relationship:

$$\sum_{k=0}^{M-1} \frac{Q_k}{P_k} = 1. \quad (3.6)$$

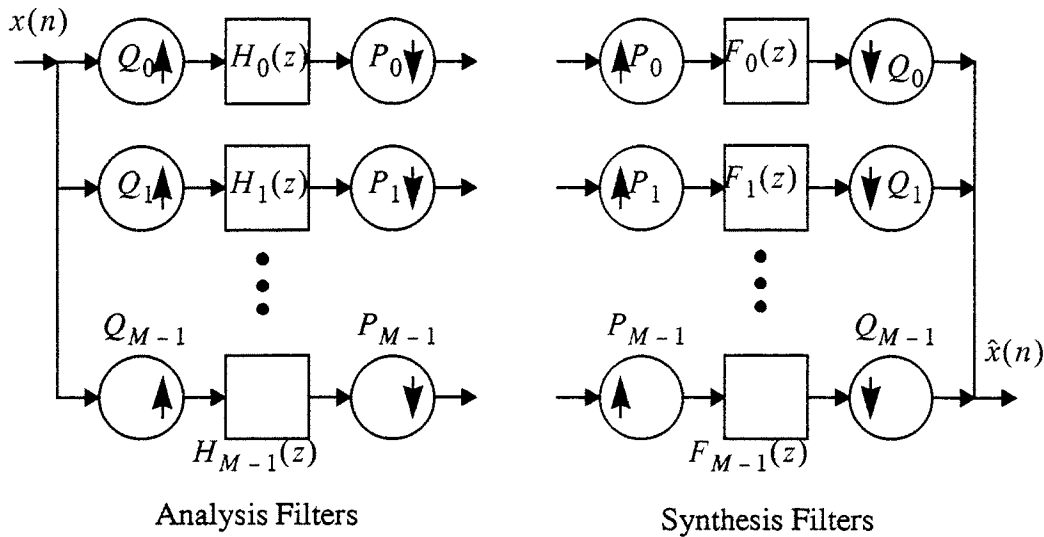


Figure 3.2 An M -band Analysis-Synthesis Non-Uniform Filter Bank with Rational Decimation Factors. After [Ref. 9].

1. FIR Power Symmetric Filter Bank

Using Equation 3.3, the aliasing cancellation condition, Equation 3.4 can be rewritten as

$$\hat{X}(z) = \frac{1}{2}[H_0(z)H_1(-z) - H_1(z)H_0(-z)]X(z) \quad (3.7)$$

Assume that $H_0(z)$ is power symmetric, that is

$$\tilde{H}_0(z)H_0(z) + \tilde{H}_0(-z)H_0(-z) = 1 \quad (3.8)$$

where the ‘ \sim ’ represents “paraconjugation” (defined by Vaidyanathan [Ref. 3] as conjugation of the function’s coefficients and replacement of z with z^{-1}). With $H_0(z)$ satisfying Equation 3.8, the filter, $H_1(z)$, is chosen as

$$H_1(z) = -z^{-N}\tilde{H}_0(-z) \quad (3.9)$$

where N is some odd number. The remaining filters can be derived as follows:

$$\begin{aligned} F_0(z) &= z^{-N}\tilde{H}_0(z) \\ F_1(z) &= z^{-N}\tilde{H}_1(z) \end{aligned} \quad (3.10)$$

Now only the filter, $H_0(z)$, remains to be designed. The power symmetric property means that the zero-phase filter, $H(z) = \tilde{H}_0(z)H_0(z)$, is a half-band filter. The design steps for the real coefficient case, where $h_0(n)$ is real, are as follows:

- Step 1. Design a zero-phase FIR half-band filter, $G(z) = \sum_{n=-N}^N g(n)z^{-n}$.
- Step 2. Define $H(z) = G(z) + \delta$, where δ is the peak stopband ripple of $G(e^{j\omega})$ to ensure that $H(e^{j\omega})$ is nonnegative.
- Step 3. Compute $H_0(z)$ as a spectral factor of $H(z)$ [Ref 3].

Figure 3.3 shows an example of perfect reconstruction filter bank design. Since the zero-phase FIR half-band filter, $G(e^{j\omega})$, is real, $H(e^{j\omega})$ is obtained by lifting the response $G(e^{j\omega})$ by δ . This is demonstrated in Figure 3.3(a).

The zero-phase FIR filter, $G(z)$, is designed using MATLAB function “*REMEZ*”, which uses the McClellan-Parks algorithm. The nonnegative zero-phase filter, $H(z)$, is also demonstrated in Figure 3.3(a). It is clear that $H(e^{j\omega}) \geq 0$ for all ω , so it is possible to find a spectral factor, $H_0(z)$, of $H(z)$.

The frequency response and the zero location of perfect reconstruction filter banks, $H_0(z)$ and $H_1(z)$ (filter length of 9, $M=2$), are shown in Figures 3.3(b) and 3.3(c), respectively. The passband gain is unity, the stopband gain is 8.5dB, and the cutoff frequency is $\pi/2$ radians. As demonstrated in Figure 3.3(c), the spectral factor, $H_0(z)$, of the filter, $H(z)$, is not unique because the zeros of $H(z)$ can be grouped into those of $H_0(z)$ and $\tilde{H}_0(z)$ in many ways.

2. Perfect Reconstruction Uniform and Non-Uniform Filter Banks

Both uniform and non-uniform filter banks are used here for the analysis and synthesis filter banks in order to obtain the desired subband signals. The proper combination of these filter banks provides flexibility in generating subband signals. The desired portions of a given signal can be filtered into narrow, non-uniform subbands, and the remaining portions of the signal can be filtered into larger, uniform subbands by selecting proper non-uniform filter banks and uniform filter banks respectively.

A perfect reconstruction, maximally decimated analysis-synthesis system based on uniform filter banks is designed as shown in Figure 3.4. The corresponding synthesis filter bank can easily be designed from the analysis filter bank.

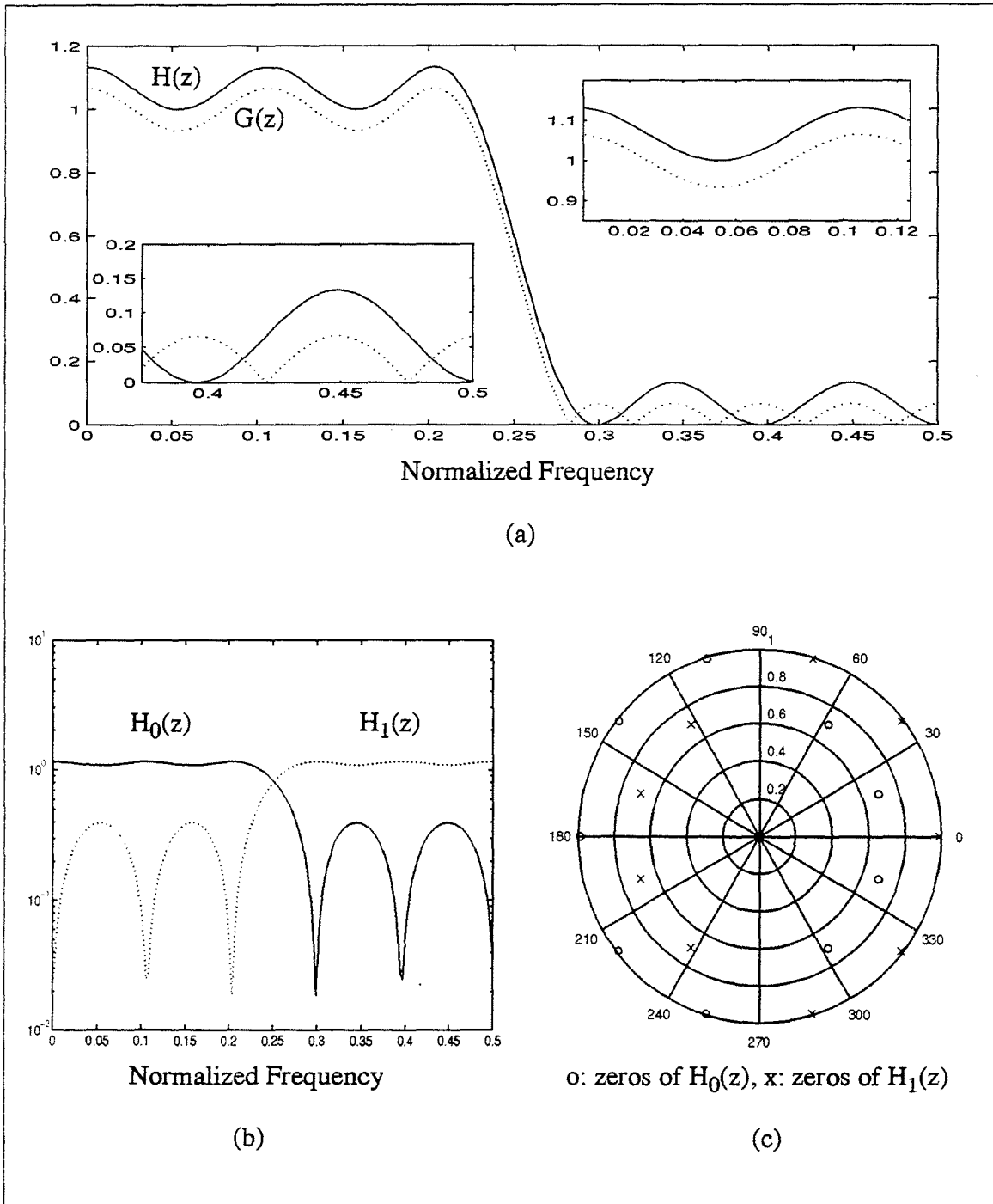


Figure 3.3 Perfect Reconstruction FIR Power Symmetric Filter Bank (Filter Order=9, M=2): (a) Zero-Phase FIR Half-band Filter $H(z)$, (b) Perfect Reconstruction FIR Filter Bank and (c) Zeros of Analysis Filter $H_0(z)$ and $H_1(z)$.

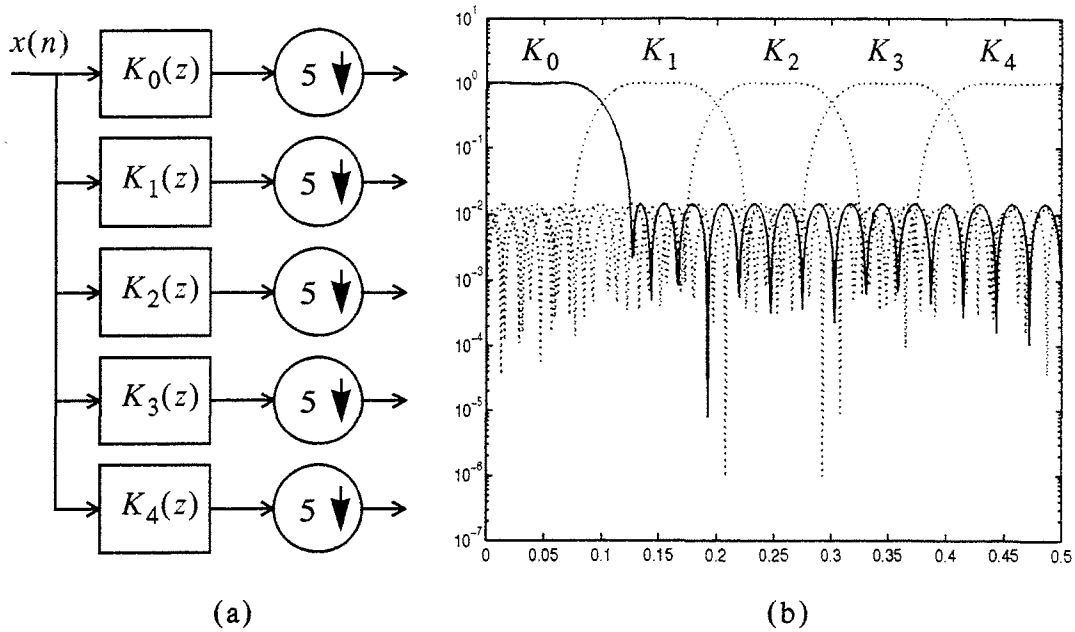


Figure 3.4 Perfect Reconstruction Uniform Analysis Filter Bank (Filter Order=35, $M=5$):

(a) Block Diagram and (b) Frequency Response.

The frequency response of a non-uniform filter bank with integer downsampling rate is shown in Figure 3.5. This non-uniform system can have a number of different forms and structures. However, for non-uniform filter banks, the decimation factors, D_k , $k = 0, \dots, M - 1$, have the following constraint

$$\sum_{k=0}^{M-1} \frac{1}{D_k} = 1 \quad (3.11)$$

The synthesis filter banks of both uniform and the non-uniform kind also can easily be obtained from Equation 3.9 in that

$$F_k(z) = z^{-N} \tilde{H}_k(z) \quad (3.12)$$

where $F_k(z)$ and $H_k(z)$ are the synthesis and analysis filter bank, respectively, $k = 0, \dots, M - 1$.

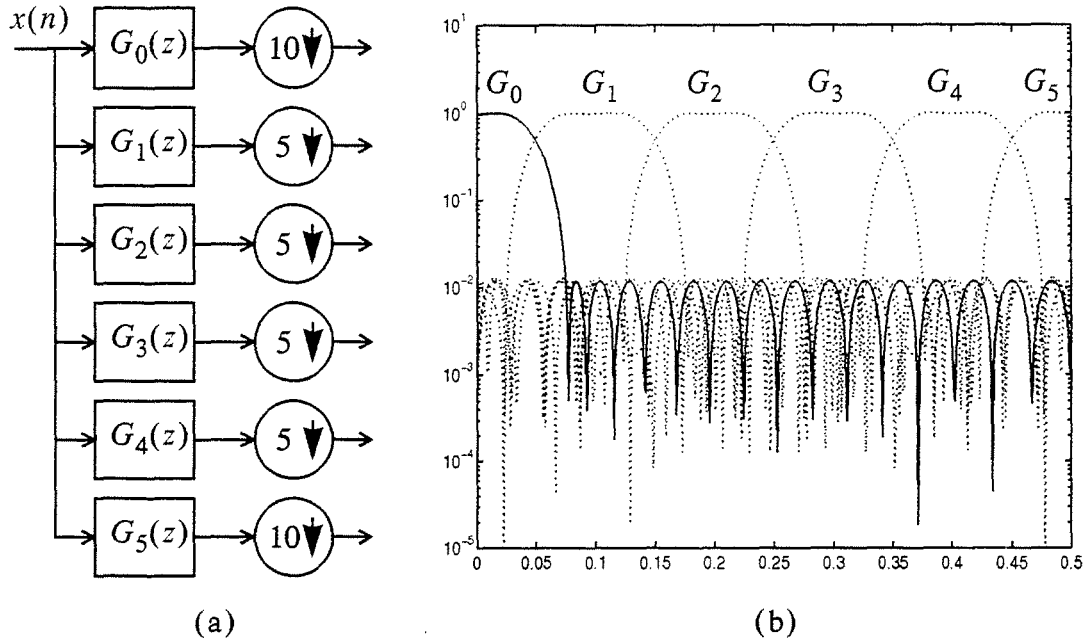


Figure 3.5 Perfect Reconstruction Non-Uniform Analysis Filter Bank (Filter Order=35, $M=6$): (a) Block Diagram and (b) Frequency Response.

3. Tree Structured Filter Bank

Both uniform and non-uniform filter banks were arranged into a tree structured analysis and synthesis filter banks to synthesize two signals obtained from different measurement devices. In this scheme, each input signal is divided into smaller, more manageable subband signals which retain the frequency characteristics of the original signal. They are then summed to obtain a wideband signal, which covers the entire

frequency area and retains the basic spectral properties of the original signals.

The overlapped portions of the two signals are not handled separately in the section. The study of overlapped portion will be presented in section IV. As mentioned in Section II, frequency concatenation methods were applied in this section using tree structured filter banks to produce a desired signal. Equation 2.11 is applied to weigh the high frequency portion of CSW data.

After decimation in a subband, a minimum data length of three times the filter order is required in order for the filtering operation to properly occur at the next tree level; a proper data length is required to minimize the end-point transients that occur during the filtering process [Ref. 2]. In the overlapping frequency band of 80 - 100 MHz, for example, the input is decimated by a factor of 50, which means that only 82 samples are present in this subband. For a filter order of 35, at least 105 points are required in this subband. To overcome this problem, a “zero-padding” method [Ref. 2] was implemented whenever the data points fell short of the required length.

Four tree-structured filter banks were designed to obtain a synthesis signal: concatenation at 80 MHz, concatenation at 100 MHz, concatenation at 80 MHz with (4/5, 1/5) system, and symmetric overlap at 90 MHz. The perfect reconstruction FIR power symmetric filter bank was applied in the case of overlap at 90 MHz. The FIR power symmetric filter bank provides perfect reconstruction of the data, so it performs better than truncation by providing a smooth transition between the HPW and the CSW spectra.

Figure 3.6 shows the schematic diagram for the filter bank, which takes HPW data up to 90 MHz and CSW data from 90 MHz to 1000 MHz as shown in Figures 3.6 and 3.7; the frequency response of the power symmetric filter bank around 90 MHz is shown in Figure 3.8. Figure 3.9 shows the results obtained from the tree structured filter bank with symmetric overlap at 90 MHz.

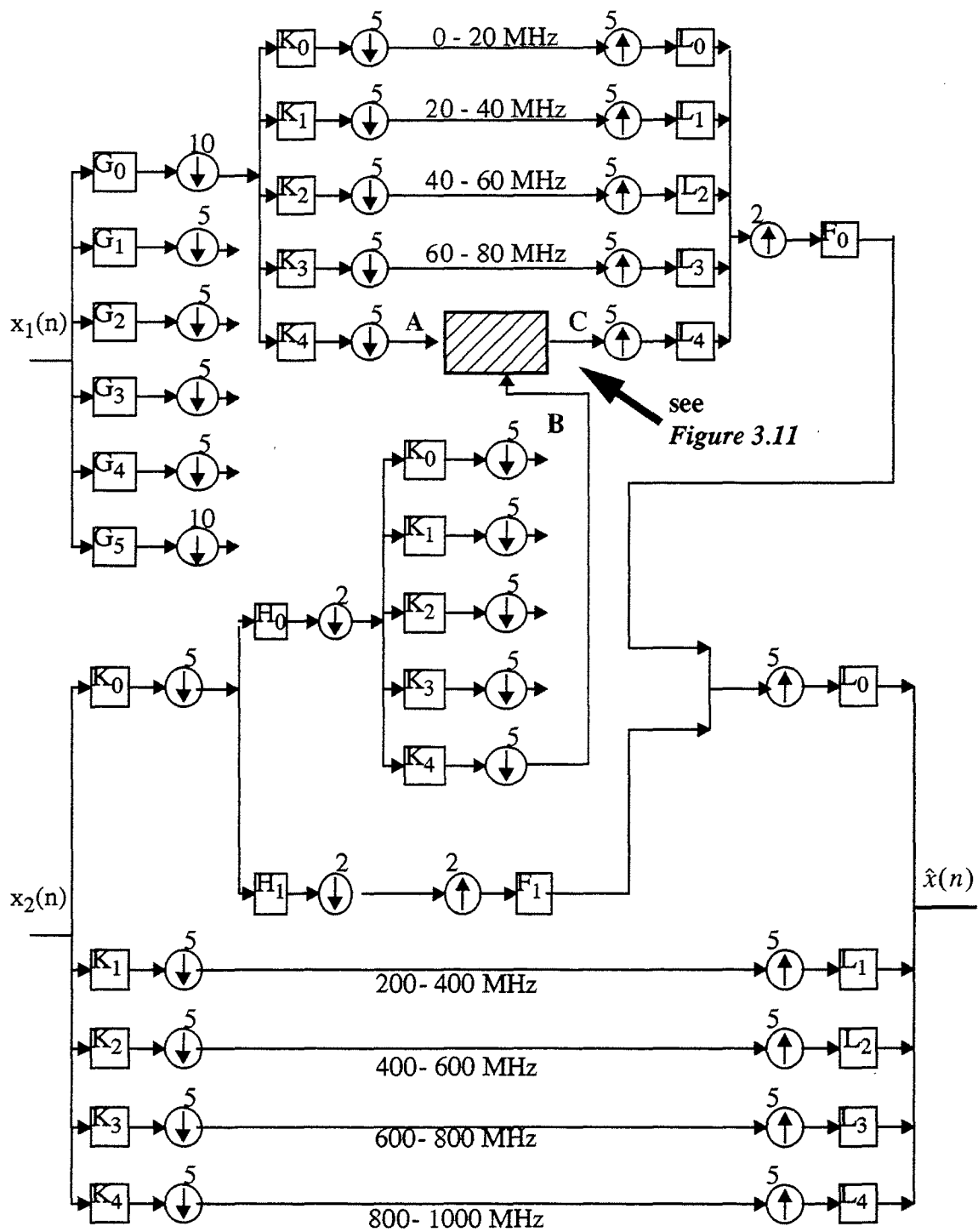


Figure 3.6 Analysis and Synthesis Tree Structured Filter Bank with Power Symmetric
Overlap at 90 MHz.

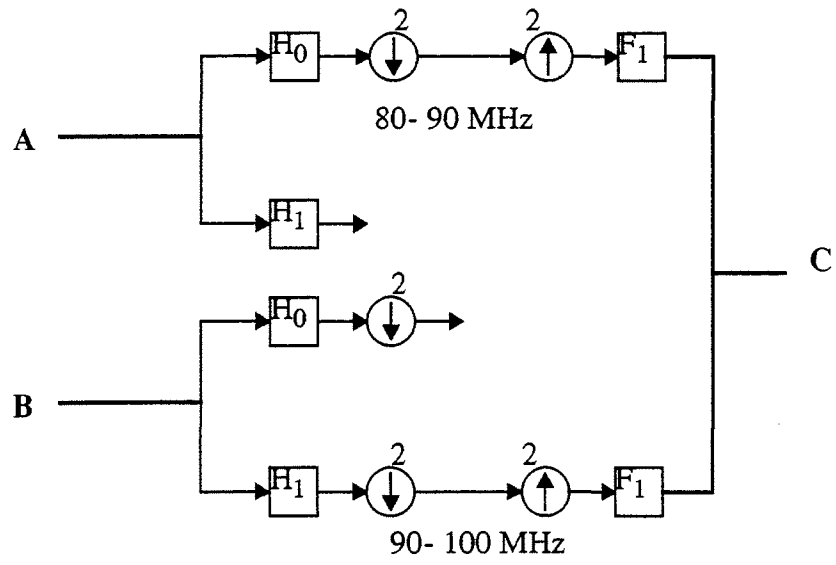


Figure 3.7 Analysis and Synthesis Tree Structured Filter Bank with Symmetric Overlap at 90 MHz: Level A and B through C.

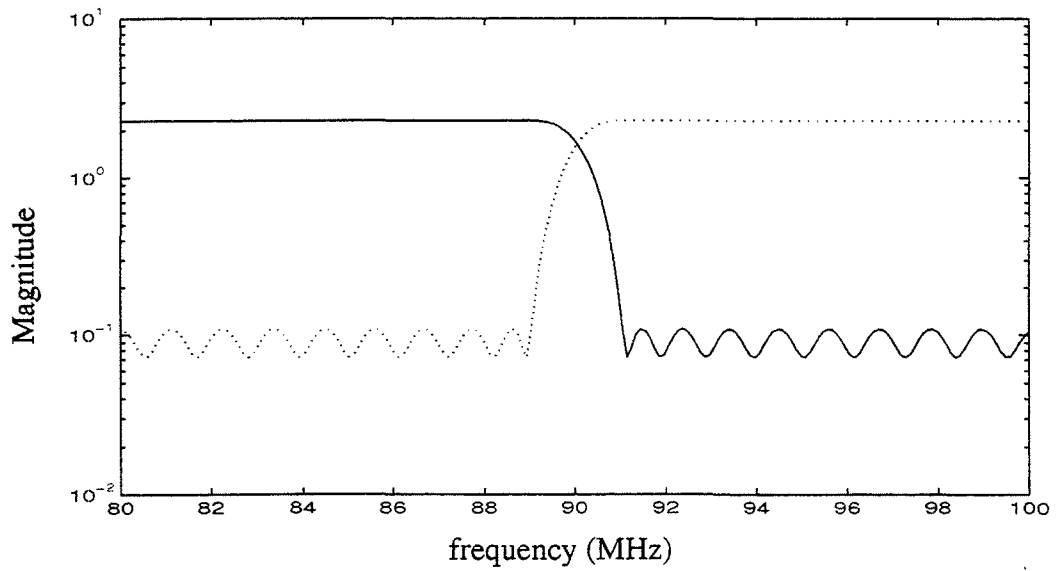


Figure 3.8 Frequency Response of Tree-Structured Filter Bank with Symmetric Overlap at 90 MHz (Filter Order = 35).

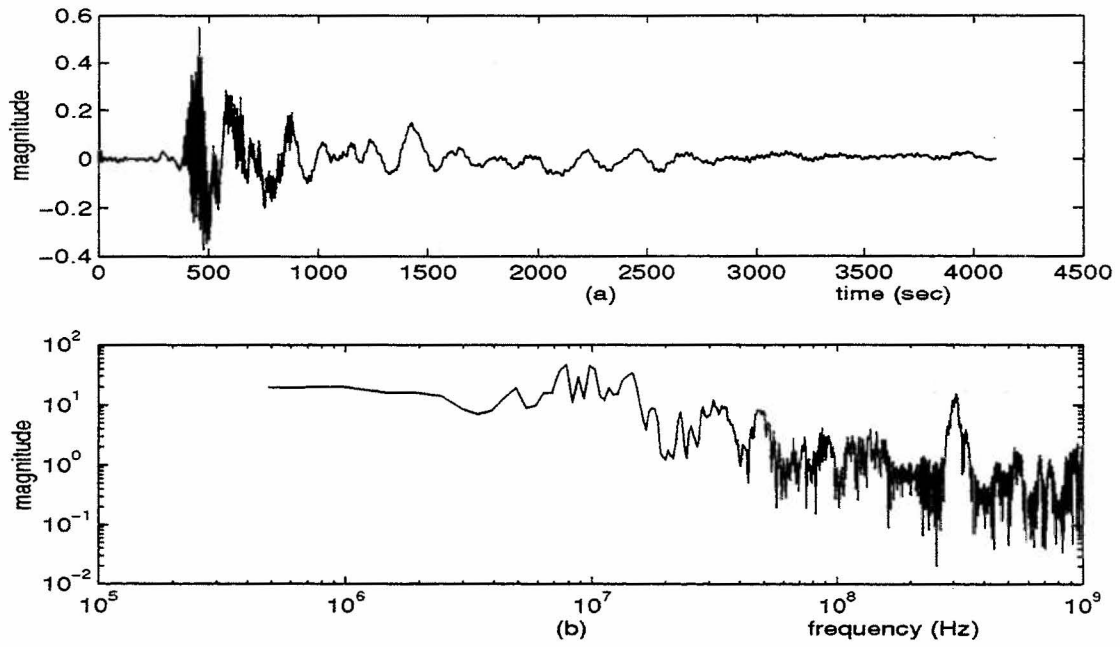


Figure 3.9 Tree-Structured Filter Bank with Symmetric Overlap at 90 MHz: (a) Time Domain Waveform and (b) Magnitude Spectrum.

IV. WIDEBAND ANALYSIS RESULTS

In this section, the sinusoidal modeling algorithm, the bandpass IFFT, and the tree-structured filter bank techniques are used to combine four different waveforms at a single test point to produce a synthesized test point signal.

1. Sinusoidal Modeling Algorithm (SMA)

The sinusoidal modeling technique implemented in this section was originally developed by McAulay and Quatieri [Ref. 10] for speech signal processing, which is transient in nature and stationary for only a short interval of time.

The block diagram illustrating the SMA is shown in Figure 4.1. In the analysis section, the input data are sectioned off into equal length frames and weighted with Hamming window. Frames are formed allowing for overlap of data. The short-time Fourier transform (STFT) approach is used to obtain the amplitudes, frequencies and phases of the sine waveforms in each spectral bin.

The frequency values are determined by first locating the peaks in the periodogram, and then matching these with peaks in adjacent frames. These peaks need not occur at the same spectral bin but are constrained to lie within some matching interval. In the synthesis part (see Figure 4.1(b)), a corresponding linear amplitude interpolation and a phase unwrapping and interpolation between matching peaks are performed. For each set of matching peaks, a sine wave is generated and amplitude modulated. The resulting sine waves are then summed to produce the synthesized waveform. For more details on this algorithm, see McAulay and Quatieri [Ref. 10].

We have used the following parameters for the sinusoidal modeling algorithm: a

FFT size of 512 and a frame length of 256 were chosen to obtain proper bin width and frequency resolution; an overlap interval of 128 was chosen for 50% overlap; a matching window size of 3 was chosen to ensure smooth frequency track; and a peak threshold of

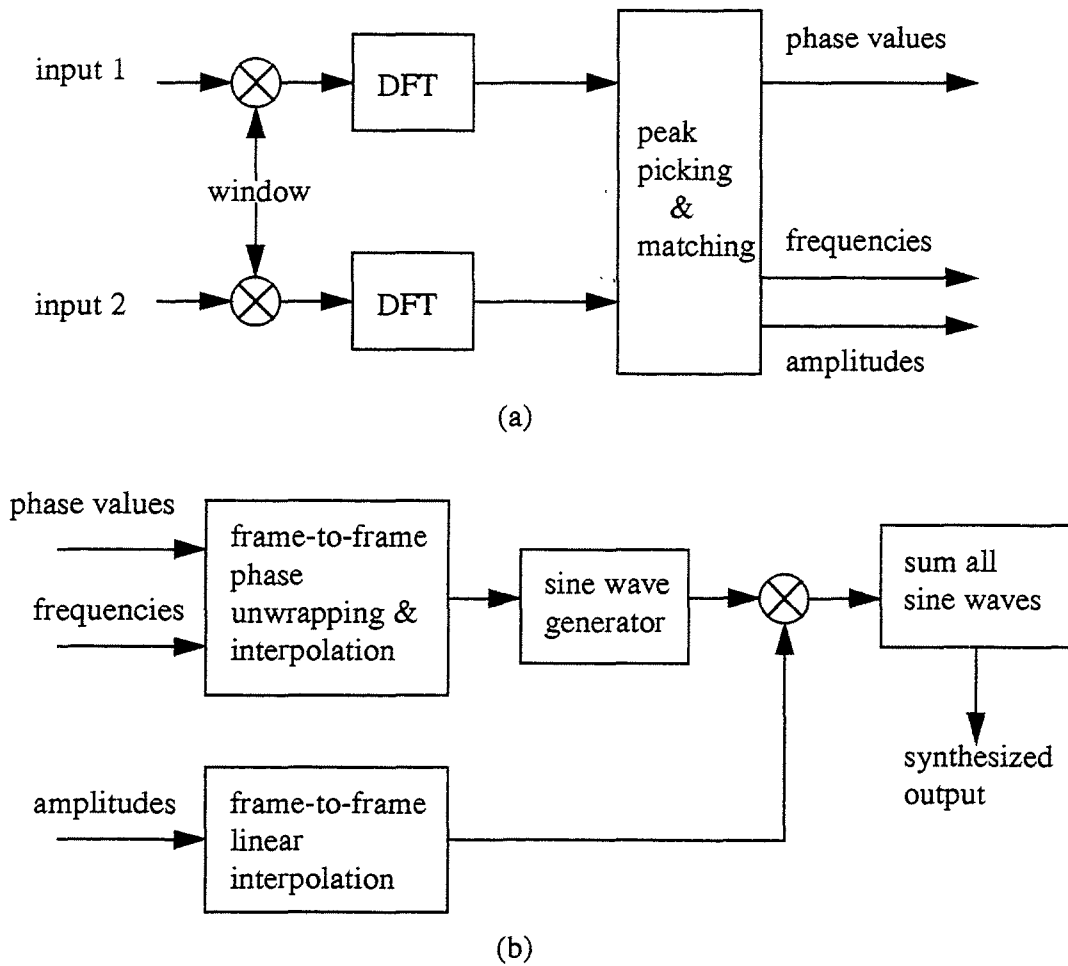


Figure 4.1 Block Diagram of the Sinusoidal Modeling Algorithm: (a) Analysis and (b) Synthesis System.

30 dB was chosen to reject weak spectral components and others due to noise [Ref. 1].

2. Combination of waveforms from different orientations

In sections II and III, to test the various algorithms, only the data from A (parallel) orientation were considered. The B (perpendicular) orientation data will now be analyzed to combine them into one waveform. There are two different sets of waveform data at each test point: HPW parallel and HPW perpendicular; and CSW parallel and CSW perpendicular.

Figures 4.2 and 4.3 show the four waveforms measured at test point I01001. Figure 4.2 shows the two HPW waveform and their spectra. The B (perpendicular) orientation spectrum shows a large low frequency coupling below the 6 MHz frequency area. The frequency content in the frequency band of 6 - 100 MHz is different for the two waveforms. The time resolution and the sampling frequency for both TAI01001 (parallel) and TBI01001 (perpendicular) orientation waveforms are given in Table 4.1. The sampling periods are slightly different; however, in this work, we have treated them to be the same; we have used $\Delta t = 0.4674 \times 10^9$ (sec), which is from TAI01001.

Table 4.1: HPW Waveforms at Test Point I01001

	TAI01001	TBI01001
Number of Data Point	4096	4096
Sampling Period, Δt (sec)	0.4674e-9	0.4629e-9
Sampling Frequency, f_s (Hz)	2.1394e9	2.1603e9
Bin Width, Δf (Hz)	5.2231e6	5.2742e6

Figure 4.3 shows the originally recorded frequency domain CSW data and its time domain representation at test point I01001. The frequency content of the two waveforms is different. It is more obvious at lower frequencies (< 10 MHz).

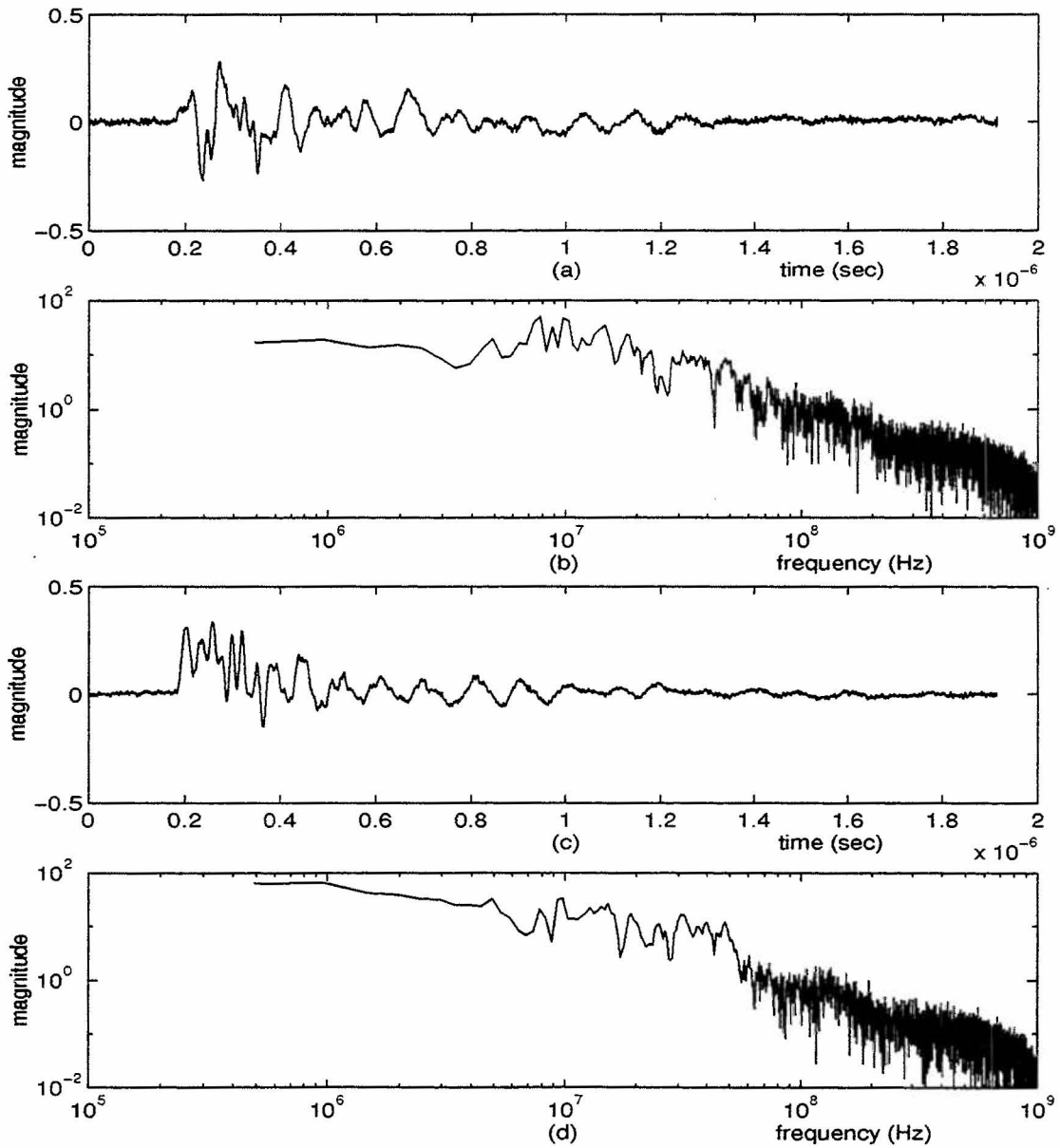


Figure 4.2 HPW Data: (a)-(b) Time Domain Waveform and Magnitude Spectrum of TAI01001; (c)-(d) Time Domain Waveform and Magnitude Spectrum of TBI01001.

The two waveforms are analyzed using the short-time Fourier transform (STFT) approach, which yields a set of frequencies, magnitudes and phases for each waveform. The

two sets of analysis data are input to the peak picking block (see Figure 4.1(a)) of the

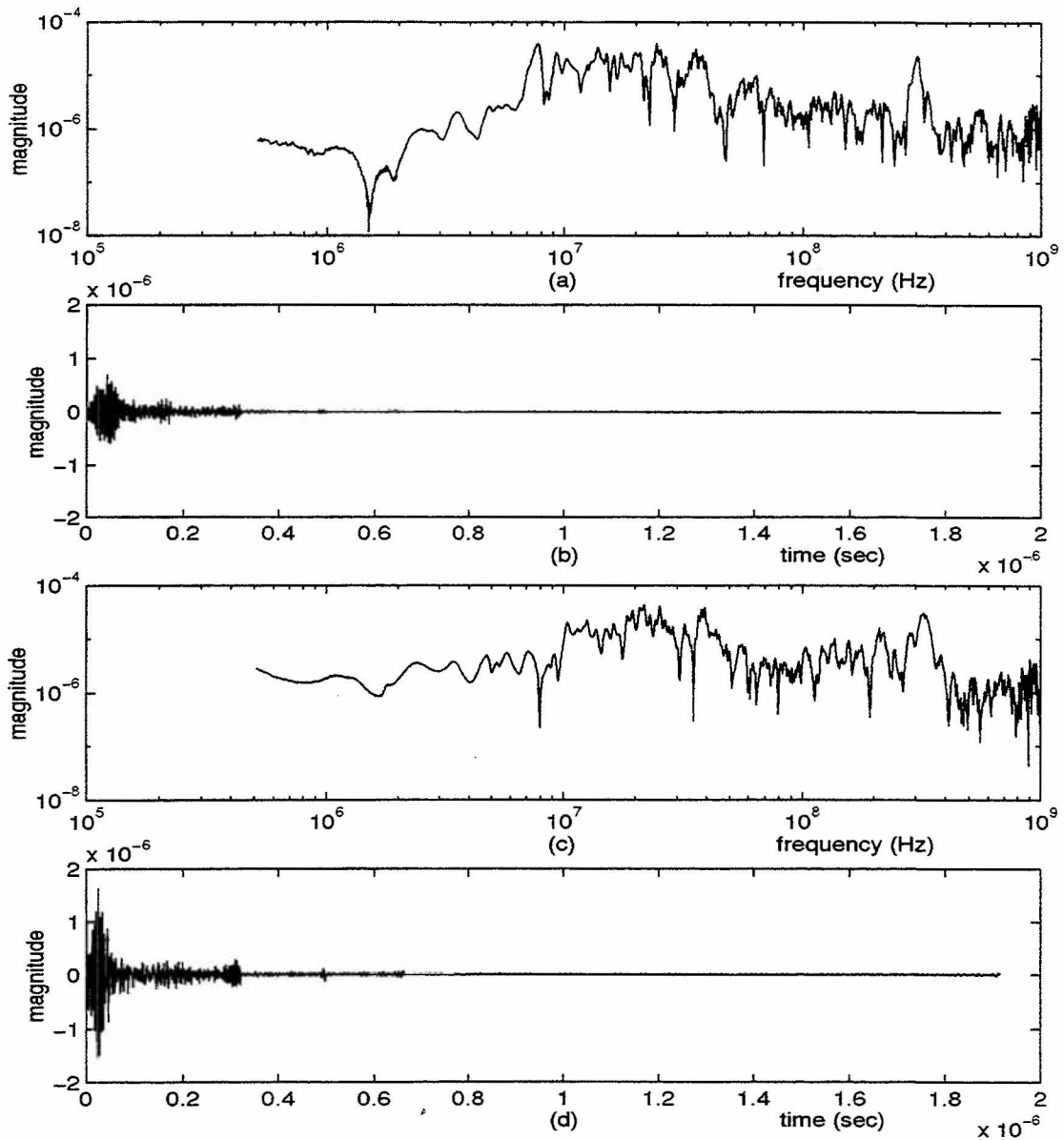


Figure 4.3 CSW Data: (a)-(b) Magnitude Spectrum and Time Domain Waveform of LAI01001; (c)-(d) Magnitude Spectrum and Time Domain Waveform of LBI01001.

SMA algorithm. For a given sinusoidal frequency, the peak picking algorithm tries to match the spectral peaks in the two spectra. The spectral peaks and the corresponding phases are then input to the synthesis part of the algorithm (see Figure 4.1(b)).

Figure 4.4 shows the plots of TAI01001 (parallel) and TBI01001 (perpendicular) orientation waveforms and the combined waveform obtained using the sinusoidal modeling algorithm. Figure 4.5 shows the plots of LAI01001 (parallel) and LBI01001 (perpendicular) orientation waveforms and the combined waveform obtained using the sinusoidal modeling algorithm. Before the CSW waveforms are combined, they were time shifted. The time shift was necessary to ensure the same sequence of windowing on both HPW and CSW data. Figure 4.5 shows the plots of LAI01001 (parallel) and LBI01001 (perpendicular) orientation waveforms and the combined waveform obtained using the sinusoidal modeling algorithm.

3. Synthesis of Transient Waveform from Four different Data Sets

In this section, techniques developed in Sections II and III are applied to combine the HPW and the CSW waveforms synthesized in the previous section. The result is a synthesized test point waveform obtained as a combination of measurements from two different orientations and two different spectral ranges. Here, we use the bandpass IFFT, multirate filter banks, and the SMA algorithm to obtain the synthesized test point waveform. Results of the two techniques are presented for the case where the concatenation takes place at 90 MHz for the bandpass IFFT technique and the power symmetric overlap takes place over a 2 MHz frequency range around 90 MHz for the filter bank technique.

In the first method, the bandpass IFFT method with spectral concatenation at 90 MHz is used. First, the HPW and the CSW waveforms from the same orientation are

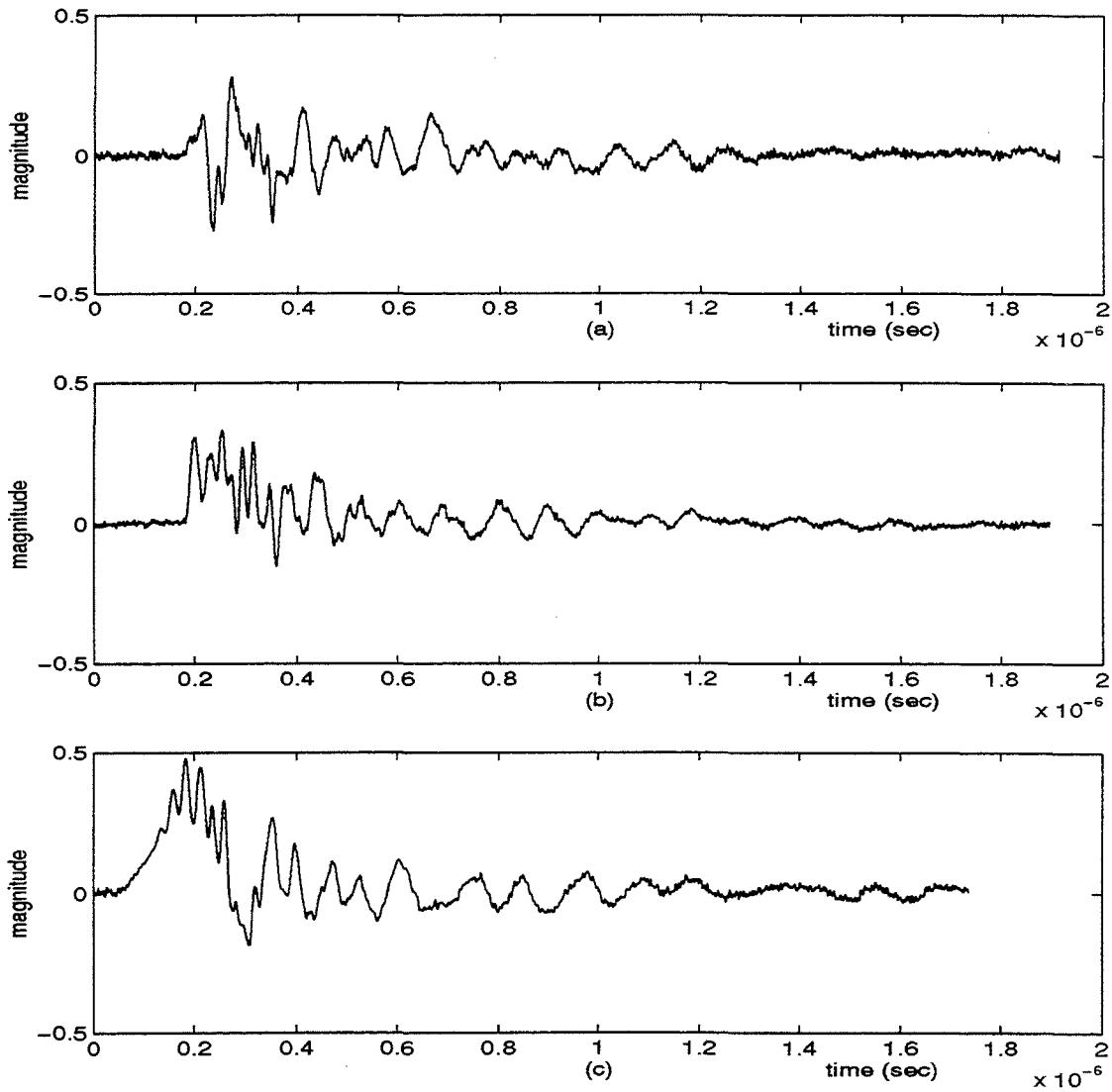


Figure 4.4 Sinusoidal Modeling Algorithm Applied to the HPW Waveforms: (a) TAI01001 (b) TBI01001 and (c) Combined Waveform.

combined into a single synthesized waveform using the spectral concatenation technique (developed in Section II) at 90 MHz. Then, the two synthesized waveforms (from A and B orientations) are combined using the SMA algorithm to obtain the final synthesized test

point waveform. In the second method, the tree-structured filter bank method (developed in Section II) with power symmetric overlap around 90 MHz is used with the same sequence of operations as in the first method. Results of the two methods are presented in Figures 4.6 and 4.7. The time and frequency domain representations of the synthesized test point waveform obtained from the two methods are included in Figure 4.8, so the two final waveforms can be visually compared.

4. Norm Attribute Measurement Results

In this section, we use the norm attribute measure [Ref. 11] in an attempt to provide a means of quantitative comparison. A norm attribute, N , of a time domain waveform, $f(t)$, is written as [Ref. 11]

$$N = \|f(t)\| \geq 0. \quad (4.1)$$

The norm attribute is a scalar having the following properties:

$$N = 0 \quad \text{if and only if} \quad f(t) \equiv 0, \quad \text{for all } t \quad (4.2)$$

$$\|Af(t)\| = |A|\|f(t)\|, \quad A \text{ is any scalar} \quad (4.3)$$

$$\|f_1(t) + f_2(t)\| \leq \|f_1(t)\| + \|f_2(t)\| \quad (\text{triangle inequality}) \quad (4.4)$$

Table 4.2 includes the definitions for a set of five norm attributes which are believed to capture the important features of electromagnetic transient waveforms. For a detailed discussion of the five norm attributes, see Thomas and Lubell [Ref. 11].

The first norm, N_1 , is the peak amplitude of the waveform (in this case magnitude

of current). The second norm, N_2 , is the peak value of the derivative of the waveform. The

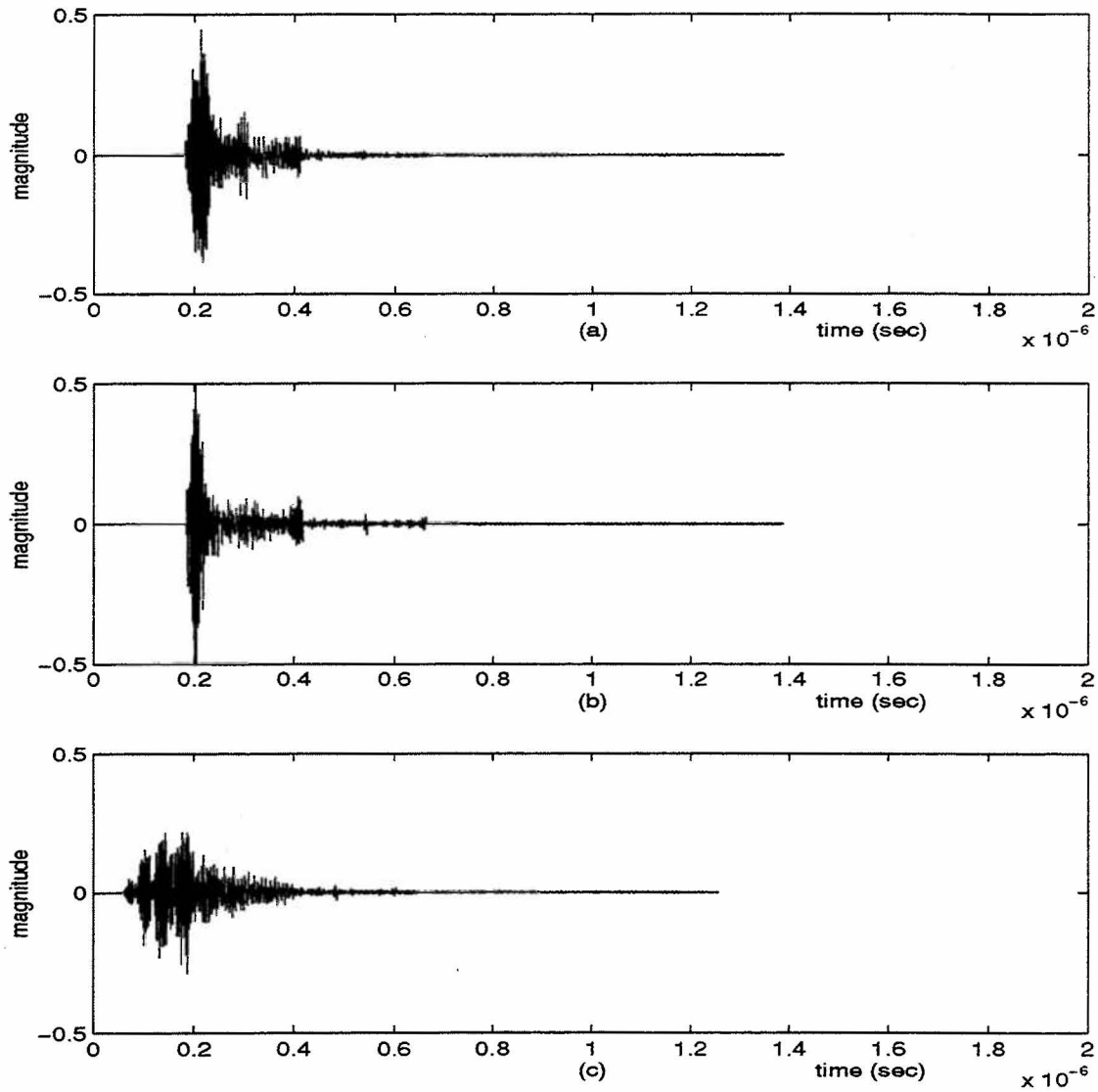


Figure 4.5 Sinusoidal Modeling Algorithm Applied to the CSW Waveforms: (a) LAI01001 (b) LBI01001 and (c) Combined Waveform.

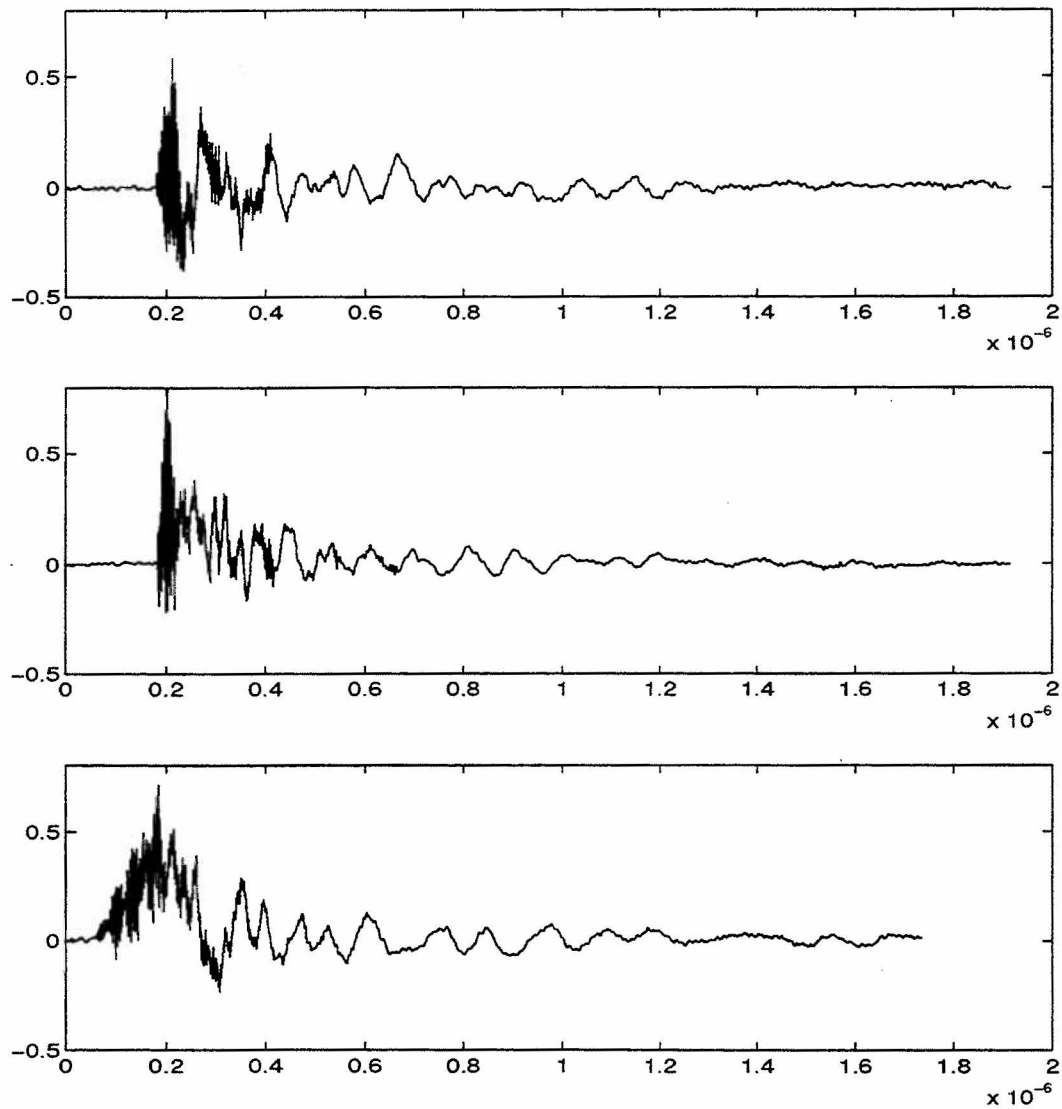


Figure 4.6 Bandpass IFFT with Concatenation at 90 MHz: (a) Synthesized Time Domain Waveform of TAI01001 and TBI01001; (b) Synthesized Time Domain Waveform of LAI01001 and LBI01001; and (c) Synthesized Test Point Waveform.

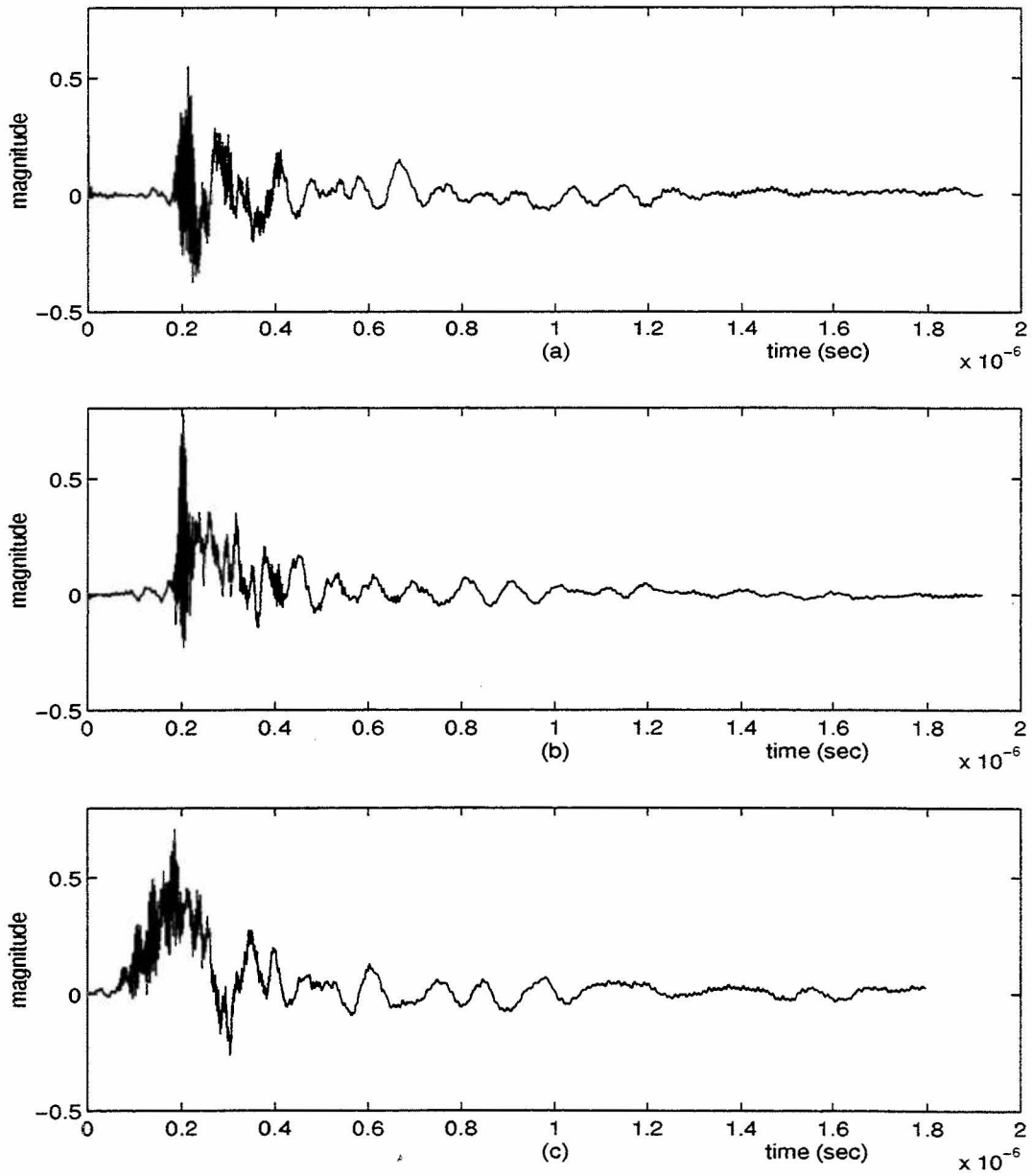


Figure 4.7 Filter Bank with Symmetric Overlap around 90 MHz: (a) Synthesized Time Domain Waveform of TAI01001 and LAI01001; (b) Synthesized Time Domain Waveform of TBI01001 and LBI01001; and (c) Synthesized Test Point Waveform.

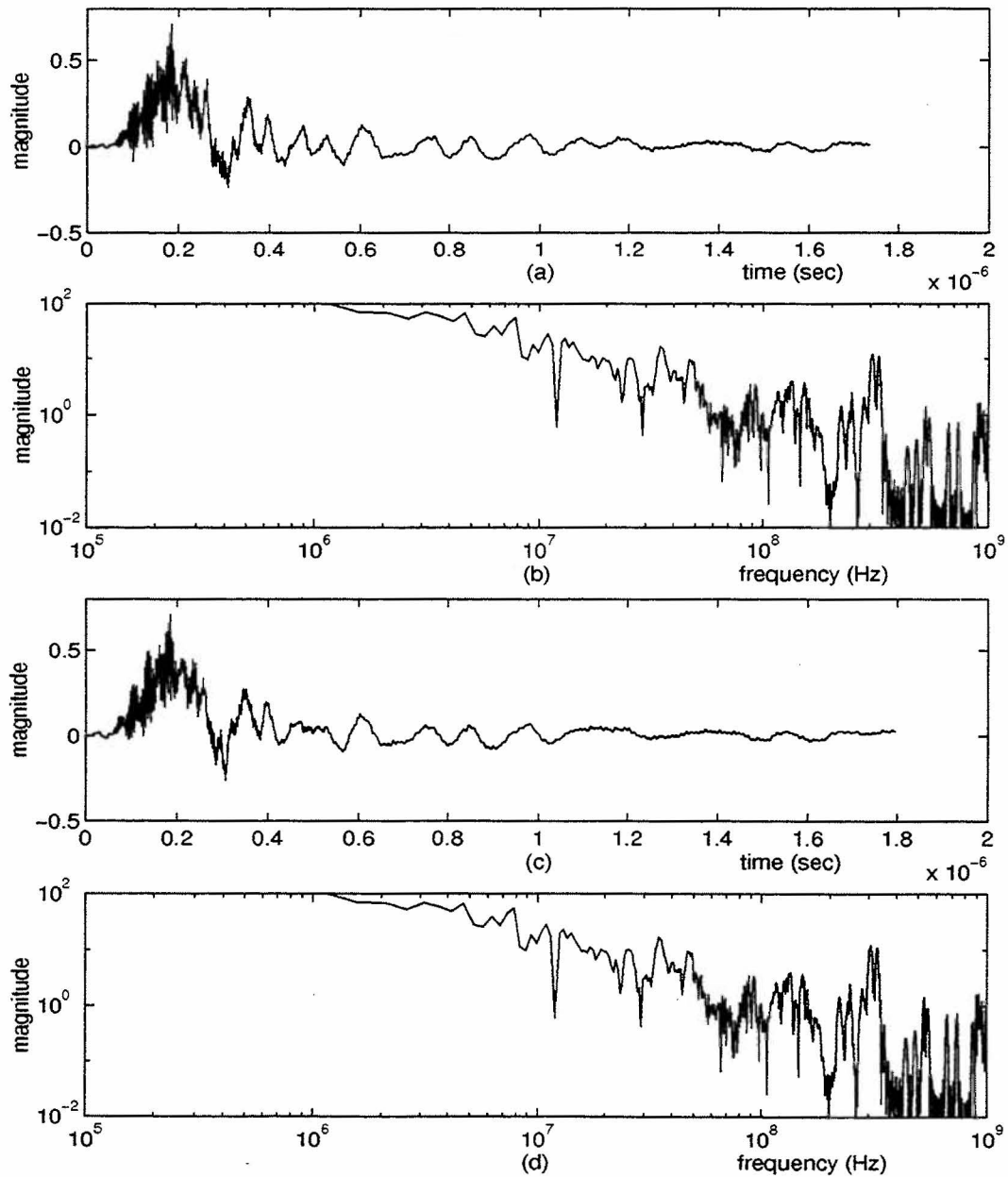


Figure 4.8 Synthesized Test Point Waveforms: (a) Time-domain and (b) Frequency-domain Representations using the Bandpass IFFT with Concatenation at 90 MHz; (c) Time-domain and (d) Frequency-domain Representations using the Filter Bank with Symmetric Overlap around 90 MHz.

third norm, N_3 , is the peak impulse and measures the peak charge for current measurements. The fourth norm, N_4 , measures the total area of the waveform, and the fifth norm, N_5 , measures the waveform energy [Refs. 1 and 11].

These norm attributes are used to determine whether the synthesized test

Table 4.2: Norm Attributes, After [Ref. 11]

Norm Quantity	Norm Attribute	Feature of $f(t)$
$N_1 = f(t) _{\max}$	Peak Amplitude	Amplitude
$N_2 = df(t)/dt _{\max}$	Peak Derivative	Variation
$N_3 = \left \int_0^t f(x) dx \right _{\max}$	Peak Impulse	Content
$N_4 = \int_0^{\infty} f(x) dx$	Rectified Impulse	Content
$N_5 = \left[\int_0^{\infty} f^2(x) dx \right]^{1/2}$	Root Action Integral	Content

pointwaveform retains the largest (or worst case) norm attributes from the original component waveforms. The norm attributes of the component waveforms and the synthesized test point waveform for test point I01001 are listed in Table 4.3 and 4.4 for the bandpass IFFT method and the filter bank method, respectively. From Table 4.3, both methods produce the norm attributes that are very close. Except for N_4 , the other norm values of the synthesized test point waveform are close to the maximum values of the component waveforms. Comparison over the overlapped region, from Table 4.4, indicates that the filter bank technique produces norm values that are closer to the maximum norm values of the component waveforms.

Table 4.3: Norm Attribute Comparison of Waveforms (Test Point I01001)

Norm Attribute	Component Waveforms				Synthesized Test Point Waveforms	
	TA 01001	TB 01001	LA 01001	LB 01001	Bandpass IFFT	Filter Bank
Peak Amplitude	0.5760 e-6	0.5480 e-6	0.0660 e-6	0.0390 e-6	0.3900 e-6	0.3890 e-6
Peak Derivative	0.2125 e+8	0.2139 e+8	4.1121 e+8	4.9478 e+8	2.7869 e+8	2.3438 e+8
Peak Impulse	0.0193 e-6	0.0900 e-6	0.0005 e-6	0.0006 e-6	0.1227 e-6	0.1561 e-6
Rectified Impulse	0.5630 e-6	0.6250 e-6	0.0780 e-6	0.0410 e-6	0.0040 e-6	0.0040 e-6
Root Action Integral	0.2837	0.3382	0.4460	0.5682	0.5022	0.5032

Table 4.4: Norm Attributes for 80- 100 MHz Overlap (Test Point I01001)

Norm Attribute	Component Waveforms				Synthesized Test Point Waveforms	
	TA 01001	TB 01001	LA 01001	LB 01001	Bandpass IFFT	Filter Bank
Peak Amplitude	0.6500 e-7	0.3100 e-7	0.0500 e-7	0.0100 e-7	0.0500 e-7	0.0100 e-7
Peak Derivative	0.9768 e+8	0.7755 e+8	7.3808 e+8	4.7091 e+8	2.3151 e+8	1.5225 e+8
Peak Impulse	0.7016 e-9	0.1897 e-9	0.7734 e-9	0.4017 e-9	0.5921 e-9	0.1272 e-9
Rectified Impulse	0.6700 e-7	0.3000 e-7	0.0700 e-7	0.0200 e-7	0.0600 e-7	0.0200 e-7
Root Action Integral	0.0887	0.0725	0.5496	0.4017	0.1594	0.1272

V. CONCLUSIONS

In this report, the bandpass IFFT filter bank and the multirate digital filter bank techniques were developed to analyze and synthesize the component waveforms to produce a synthesized test point waveform that retains the basic properties of the component waveforms. The component waveforms were recorded by two separate measurement systems (HPW and CSW) under two different aircraft orientations (parallel and perpendicular). The HPW waveforms cover a (reliable) frequency range of 0.5-100 MHz while the CSW data are considered reliable over 80-1000 MHz. This leaves a spectral overlap between the HPW and CSW waveforms in the range of 80-100 MHz. The HPW waveforms were recorded in the time domain with a sampling period of $\Delta t = 0.4674 \times 10^9$ sec. The CSW data were recorded in the frequency domain in six separate subbands with different bin widths.

In order to produce a synthesized test point waveform, the following steps were performed. The HPW and the CSW data were transformed to be in the same domain (time or frequency) using the bandpass IFFT techniques. The sampling rates and bin widths were converted by interpolation/decimation techniques to force them to be the same for all waveforms and subbands. Data from two orientations were then combined using the SMA algorithm. Finally, the spectrally overlapped subbands were combined using spectral concatenation and symmetric overlap approaches.

The tree-structured filter bank method of wideband signal analysis provides an efficient method by dividing a wideband signal into smaller, more manageable subbands. Care should be taken to ensure that sufficient number of data points are available for a given filter order. Insufficient data length may lead to end effects in filtering. In designing filters, effort should be made to minimize side-lobe and “aliasing” effects. No technique

is available to completely eliminate the loss of information due to aliasing effect, but it can be minimized.

Since the true test point waveform could not be physically measured, it was not possible to determine the accuracy of the synthetic test waveforms produced in this work. Visual observations and norm attribute measures were used to evaluate the closeness of the synthesized test point waveform to its component waveforms. The results obtained from the bandpass IFFT and multirate filter bank methods were identical when visually compared. The norm attribute values provide a means for numerical comparison, and these values for the synthesized test point waveform were generally close to the maximum norm attribute values of the component waveforms.

REFERENCES

- [1]. Thomas F. Winnenberg, "Wideband Signal Analysis Applied to EMP Stress Waveforms," Master's thesis, Naval Postgraduate School, Monterey, California, December 1993.
- [2]. Curt E. Martin, "Wideband Signal Analysis Using Multirate Filter Banks," Master's thesis, Naval Postgraduate School, Monterey, California, December 1994.
- [3]. Vaidyanathan, P.P., "*Multirate System and Filter Banks*," Prentice Hall, Inc., Englewood Cliffs, New Jersey 1993.
- [4]. Charles W. Therrien, "*Discrete Random Signals and Statistical Signal Processing*," Prentice Hall, Inc., Englewood Cliffs, New Jersey 1992.
- [5]. Vaidyanathan, P.P., "Theory and Design of M-Channel Maximally Decimated Quadrature Mirror Filters with Arbitrary M, Having the Perfect-Reconstruction Property," *IEEE Transactions On Acoustics, Speech, and Signal Processing*, Vol.

ASSP-35, No. 4, April 1987.

- [6]. Haykin, Simon S., "*An Introduction to Analog and Digital Communications*," John Wiley and Sons, Inc., Hamilton Printing Company, New York, 1989.
- [7]. Ronard E. Crochiere and Lawrence R. Rabiner, "*Multirate Digital Signal Processing*," Prentice Hall, Inc., Englewood Cliffs, New Jersey, 1983.
- [8]. Martin Vetterli, "A Theory of Multirate Filter Banks," *IEEE Transactions On Acoustics, Speech, and Signal Processing*, Vol. ASSP-35, No. 3, March 1987.
- [9]. Kambiz Nayebi, Thomas P. Barnwell, III, and Mark J. T. Smith, "Nonuniform Filter Banks: A Reconstruction and Design Theory," *IEEE Transactions On Signal Processing*, Vol. 41. No. 3. March 1993.
- [10]. Robert J. McAulay, and Thomas F. Quatieri, "Speech Analysis/Synthesis Based on a Sinusoidal Representation," *IEEE Transactions On Acoustics, Speech, and Signal Processing*, Vol. ASSP-34, No. 4, August 1986.
- [11]. Thomas, R. E. and Lubell, J. I., "An Approach to the Development of EMP Specifications and Standards Based on Norm Attributes," Defense Nuclear Agency Technical Report DNA-TR-89-142, February 1990.

DISTRIBUTION LIST

1. Defense Technical Information Center 2
8725 John J. Kingman Road, Ste 0944
FT. Belvoir, VA 22060-6218
2. Dudley Knox Library 2
Naval Postgraduate School
Monterey, CA 93943-5101
3. Chairman, Code EC 1
Department of Electrical and Computer Engineering
Naval Postgraduate School
Monterey, CA 93943-5121
4. Samuel J. Frazier, Code 5.1.7.2 2
Aircraft Division
Naval Air Warfare Center
Patuxent River, MD 50607-5000
5. Ed Parimuha, Code 5.1.7.2 2
Aircraft Division
Naval Air Warfare Center
Patuxent River, MD 50607-5000
6. Prof. Murali Tummala, Code EC/Tu 4
Department of Electrical and Computer Engineering
Naval Postgraduate School
Monterey, CA 93943-5121
7. Prof. Gurnam S. Gill , Code EC/GI 1
Department of Electrical and Computer Engineering
Naval Postgraduate School
Monterey, CA 93943-5121
8. Prof. Ralph Hippenstiel, Code EC/Hi 1
Department of Electrical and Computer Engineering
Naval Postgraduate School
Monterey, CA 93943-5121

9. Prof. Charles W. Therrien, Code EC/Ti 1
Department of Electrical and Computer Engineering
Naval Postgraduate School
Monterey, CA 93943-5121

10. Prof. Jinok Park 1
Department of Electrical Engineering
P.O. Box 77, Gongneung-Dong, Nowon-gu, Seoul, 139-799
Republic of Korea

11. Prof. Keun-Ho Ryoo 1
Department of Electrical Engineering
P.O. Box 77, Gongneung-Dong, Nowon-gu, Seoul, 139-799
Republic of Korea

12. Captain Jeong, Soonho 1
254-8, Joongkok-dong
Kwangjin-gu, Seoul
Republic of Korea